

Review

Polyacrylic Acid Nanoplatfoms: Antimicrobial, Tissue Engineering, and Cancer Theranostic Applications

Hassan Arkaban ¹, Mahmood Barani ^{2,*}, Majid Reza Akbarizadeh ^{3,*}, Narendra Pal Singh Chauhan ⁴, Sapana Jadoun ⁵, Maryam Dehghani Soltani ⁶ and Payam Zarrintaj ⁷

¹ Department of Chemistry, University of Isfahan, Isfahan 8174673441, Iran; hassan.arkaban@gmail.com

² Medical Mycology and Bacteriology Research Center, Kerman University of Medical Sciences, Kerman 7616913555, Iran

³ Department of Pediatric, Amir Al Momenin Hospital, Zabol University of Medical Sciences, Zabol 9861663335, Iran

⁴ Department of Chemistry, Faculty of Science, Bhupal Nobles's University, Udaipur 313002, Rajasthan, India; narendrapalsingh14@gmail.com

⁵ Department of Analytical and Inorganic Chemistry, Faculty of Sciences, University of Concepcion, Edmundo Larenas 129, Concepcion 4070371, Chile; sjadoun022@gmail.com

⁶ Department of Chemistry, Faculty of Science, Yazd University, Yazd 8915818411, Iran; maryam.dehghanisoltani@gmail.com

⁷ School of Chemical Engineering, Oklahoma State University, 420 Engineering North, Stillwater, OK 74078, USA; payam.zarrintaj@gmail.com

* Correspondence: mahmoodbarani7@gmail.com (M.B.); akbarizadeh63@gmail.com (M.R.A.)

Abstract: Polyacrylic acid (PAA) is a non-toxic, biocompatible, and biodegradable polymer that gained lots of interest in recent years. PAA nano-derivatives can be obtained by chemical modification of carboxyl groups with superior chemical properties in comparison to unmodified PAA. For example, nano-particles produced from PAA derivatives can be used to deliver drugs due to their stability and biocompatibility. PAA and its nanoconjugates could also be regarded as stimuli-responsive platforms that make them ideal for drug delivery and antimicrobial applications. These properties make PAA a good candidate for conventional and novel drug carrier systems. Here, we started with synthesis approaches, structure characteristics, and other architectures of PAA nanoplatfoms. Then, different conjugations of PAA/nanostructures and their potential in various fields of nanomedicine such as antimicrobial, anticancer, imaging, biosensor, and tissue engineering were discussed. Finally, biocompatibility and challenges of PAA nanoplatfoms were highlighted. This review will provide fundamental knowledge and current information connected to the PAA nanoplatfoms and their applications in biological fields for a broad audience of researchers, engineers, and newcomers. In this light, PAA nanoplatfoms could have great potential for the research and development of new nano vaccines and nano drugs in the future.

Keywords: polyacrylic acid (PAA); synthesize; polymerizations; antimicrobial; anticancer; biosensing



Citation: Arkaban, H.; Barani, M.; Akbarizadeh, M.R.; Pal Singh Chauhan, N.; Jadoun, S.; Dehghani Soltani, M.; Zarrintaj, P. Polyacrylic Acid Nanoplatfoms: Antimicrobial, Tissue Engineering, and Cancer Theranostic Applications. *Polymers* **2022**, *14*, 1259. <https://doi.org/10.3390/polym14061259>

Academic Editor: John Vakros

Received: 12 February 2022

Accepted: 16 March 2022

Published: 21 March 2022

Publisher's Note: MDPI stays neutral with regard to jurisdictional claims in published maps and institutional affiliations.



Copyright: © 2022 by the authors. Licensee MDPI, Basel, Switzerland. This article is an open access article distributed under the terms and conditions of the Creative Commons Attribution (CC BY) license (<https://creativecommons.org/licenses/by/4.0/>).

1. Introduction

A polymer consists of macromolecules; many tiny molecules are joined via covalent connections. Polymers are the most ubiquitous biomaterials, with uses ranging from contact lenses to pharmaceutical carriers to implantation, artificial organs, tissue engineering, medical instruments, and Cancer theranostic [1]. Polymers are divided into synthetic and natural origins, and both branches have broad applications. This is owing to polymers' unusual features, which established an altogether new notion when they were first presented as biomaterials [2–4]. Polymerizations are classified according to the reactions that occur throughout the synthesis process. It can be divided into three categories: addition, condensation, and metathesis polymerization [5,6]. Over the first time, a polymer used for construction purposes was engineered to be entirely resorbed and weaken over time. This

approach was effectively implemented for the first time with catgut sutures, then afterward on bone fixation, ligament augmentation, plates, and pins, with questionable outcomes. Synthetic polymers have several characteristics, including low density, the potential to tailor aspects to various uses, water, chemical stability, and easy practicability [7].

Polyacrylic acid (PAA), formerly recognized as poly 1-carboxyethylene, is a high molecular weight synthetic (manufactured) polymer made with acrylic acid monomers. Poly (1-carboxyethylene) is a commercialized polymer at a small price. It is a biocompatible superabsorbent polymer soluble in water, nonpoisonous, and recyclable [8,9]. Superabsorbent polymers (SAP) are hydrophilic net-organized polymers like carboxylic acid, hydroxyl, and amines. Compared to typical water-absorbing polymers, superabsorbents can absorb a high volume of water and eliminate it even under pressure. Superabsorbents are extensively applied in healthcare, farming, agriculture, biomedical and everyday physiological goods, isolation techniques, and sewage treatment because of their exceptional qualities [10,11].

A stable structure can be formed by cross-linking poly (acrylic acid) [12,13]. Poly(acrylic acid), a common pH-responsive polymer [14], has typically served as a hydrophilic section for amphiphilic or amphipathic block copolymers with a variety of unique characteristics [15]. This polymer is currently sold as a soft white powder. It has the potential to generate translucent, fragile films. It is a hygroscopic polymer that can absorb and keep water molecules by absorption or adsorption from the environment. The glass transition temperature of pristine PAA is more than 100 °C. Polyacrylic acid acts as an anionic polymer in water [16]. Radiation, allyl ethers of hydrocarbons, and other chemical substances can crosslink poly (acrylic acid). At temperatures above 200 °C, PAA can also be cross-linked. Polyacrylic acid may release water and form an insoluble cross-linked network at high temperatures. The cross-linked PAA may create a gel-like structure. The case of poly (acrylic acid)-graft chitosan is an example of chemical cross-linking [17]. Block copolymers can be made by copolymerizing poly (acrylic acid) with other polymers. Various polymers, including polyacrylamide, polyethylene oxide, cellulose, and others, can form hydrogen-bonded complexes with PAA.

This artificial polymer is used for dispersion for many other purposes [18,19]. It is also utilized as a food supplement owing to low cytotoxicity. Because it is fully biodegradable, poly (acrylic acid) is of particular interest [20]. It has high adhesive strength due to its carboxylic acid activity [21]. It is also being employed in drug delivery systems [22]. It is also an eco-friendly polymer with superior mechanical strength and clarity [23,24]. As a result, PAA is employed in adhesives, coatings, homes, packaging, pharmacology, and other medical and biological industries [25]. Because of its outstanding properties and high water absorption, poly (acrylic acid), in either linear or cross-linked form, is widely used in several kinds of fake tears [26,27]. New progresses in science, bioinformatics and nanomedicine have important influence on human healthiness [28–33]. Nanotechnology is the manipulation of matter on a near-atomic scale to produce new structures, materials and devices [34–36]. The technology promises scientific advancement in many sectors such as medicine, consumer products, energy, materials and manufacturing [37–39]. The combination of nanotechnology and PPA advantages can help to develop more efficient nanocarriers. This review looked at various fascinating applications for polyacrylic acid nanoplatforms, including biological applications. The ability of this polymer to link with other materials, such as carbon nanotubes, is also under consideration.

2. Synthesis and Structure Characteristics

PAA, often known as carbomer, is an acrylic acid (AA) polymer with a carboxylic group (–COOH) on each monomer unit end is connected to the vinyl group. For its numerous carboxyl groups, poly (acrylic acid), a thermoplastic polymer, has substantial bioavailability and thus can be employed as a surface modification for biological nanomaterials [40].

Acrylic acid (propanoic acid) is a monomer that may be crosslinked to establish hydrogels with a higher moisture content capacity. This could be used as a single or multi-component structure. Acrylic acid has the general formula of $\text{CH}=\text{CH}-\text{COOH}$, and

the carboxylic acid groups make this monomer a weak acid. The proximity of carboxylic acid groups makes the hydrogel ionizable, which can help increase its ionic strength and pH sensitivity. Acrylic acid monomers are also combined with various polymers to create multiple types of hydrogels [41–43]. Acrylic acid polymerization can occur in an acid medium employing materials like chlorosulfonic acid and sulphuric acid. Furthermore, polymerization can occur in the presence of alkalis, iron salts, light, high temperatures, unpaired valence electrons in an atom, molecule, or ion, and peroxide mixtures [44].

When all carboxyl groups dissolve, PAA has a high negative charge density. Neutralization transforms the acrylic acid monomer to sodium acrylate monomer in dissolved sodium hydroxide. As a result, this polymer and poly sodium acrylate are among the most widely employed water-soluble anionic polyelectrolytes, such as dispersion compounds, superabsorbent polymers, and ion-exchange resin. As indicated in Figure 1, they are exclusively produced by radical polymerization of sodium (acrylic acid) or acrylic acid [45–47].

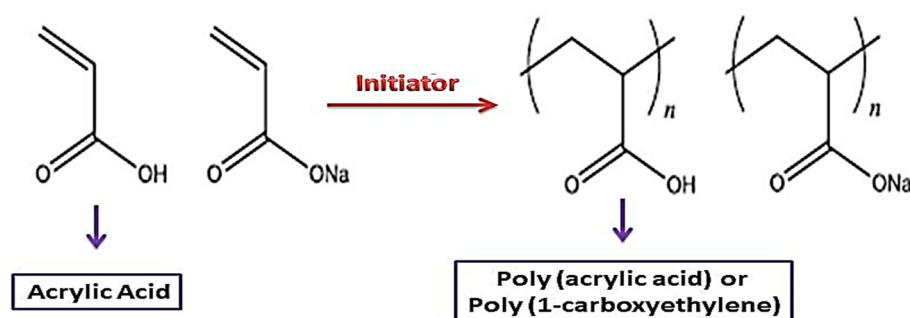


Figure 1. Synthesis and structure for poly (sodium acrylate) (NaPAA) and PAA.

The mechanical characteristics of PAA are improved by crosslinking it. Polymeric moderators in PAA might even help increase their tensile strength [48]. Furthermore, the cross-linked PAA has an incredible amount of water absorption. Poly (acrylic acid) is non-weatherable and has good optical characteristics. Various organic and inorganic nanoparticles are used to make PAA composite materials. The addition of reinforcements to the PAA network substantially impacts the final's shape, temperature resistance, mechanical characteristics, coating, and biomedical structure [49]. Combining the nanofiller with the PAA framework resulted in nanomaterials with significantly improved properties. PAA-derived nanocomposites have ushered in a slew of new technological frontiers. Adhesives, electronics, and biomedical applications all use PAA nanocomposites. Because of their unique properties and uses, PAA nanocomposites have sparked a lot of research attention. Further research should concentrate on the pattern connections in PAA-derived nanocomposites for application areas [50,51].

Because of its hydrophilic character, PAA offers higher sticking powers to objects as a stabilizing agent. The cross-linked polyacrylate can capture and hold one hundred times its weight in moisture. Propanoic acid with a high density of carboxylic groups may improve the hydrophilicity of the resultant nanocomposite or mix in biological applications. Due to its nontoxicity and absorption properties, PAA has high drug storage and delivery capabilities. The hydrophilic characteristic of PAA-based mixtures may diminish serum protein adsorption, which is desirable in some situations to reduce blood clotting. Furthermore, cross-linked PAA can be employed as a medicinal adhesive due to its excellent bonding strength. PAA has hardness and barrier qualities in film form, making it ideal for packaged food [48,52]. Poly (acrylic acid) varies its characteristics in response to changes in ionic strength and pH; for example, at $\text{pH} < 4$, precipitate occurs in aqueous solutions due to the carboxylate groups' protonation making the polymer sparsely soluble in water [53].

Different radical polymerization processes, such as inverse emulsion, have been used to make poly (acrylic acid). The developing polymer chains are not soluble in the monomer during bulk polymerization, resulting in precipitation polymerization, which poses practical issues in mixing and heat transmission. Solution polymerization is a quick

and easy way to get past these problems. To commence polymerization, redox initiation is a particularly effective method of creating free radicals under favorable circumstances. This technique is widely used in low-temperature emulsion polymerizations [54]. PAA can be made by hydrolysis of a narrowly dispersed poly (tert-butyl acrylate) (PtBA) sample, as demonstrated in Figure 2. Anionic or controlled radical polymerizations make the poly (tert-butyl acrylate) sample. Other types of PAA possessing block copolymers comprised of poly(*n*-butyl methacrylate), poly(methyl methacrylate), polystyrene (PS), and poly(2-vinyl pyridine), also polymers with a consistent branching pattern, such as star and comb polymers can be synthesized using this process [55].

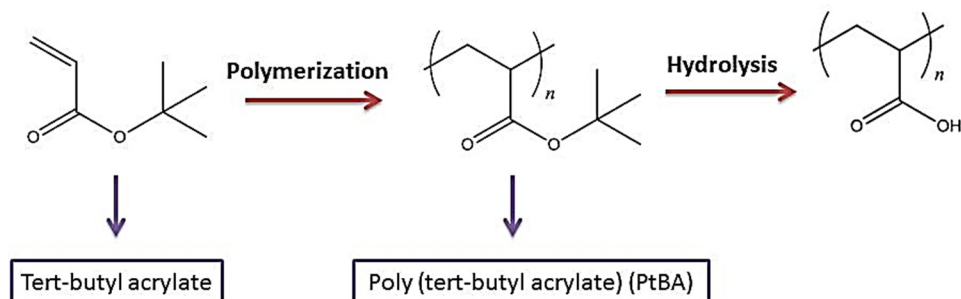


Figure 2. Synthesis for poly (sodium acrylate).

Because of its functional groups, acrylic acid is one of the monomers that can polymerize through radical polymerization. As a result, the straight production of acrylic acid by managed radical polymerization has recently become prevalent. Since AA can interact with metal, atom transfer radical polymerization (ATRP) of PAA was complex [56]. The PAA homopolymers were first produced via direct polymerization of AA in dioxane at 120 °C using nitroxide mediated polymerization (NMP) [57]. The most effective approach for targeted polymerization of AA was reversible addition-fragmentation transfer polymerization. The first straight polymerization of AA was in dimethylformamide (DMF) at low conversion. In controlled radical polymerization of AA in protic conditions, several reversible additive transfer polymerization (RAFT) compounds were examined phenoxyanthates, and dibenzyl dithiocarbonates were shown to be the most appropriate RAFT products [58]. Side reactions in the radical polymerization of acrylic monomers include chain transfer to solvent, which restricts chain transfer to polymer and high molecular weight, resulting in branching architectures [59].

In a relatively short processing time, cobalt porphyrin derivatives are used to mediate the controlled radical polymerization of AA to create PAA with a high molecular weight and minimal polydispersity [60]. Aside from the environmental benefit, the polymerization level of acrylic acid is much higher through water than in some other solvents. Loiseau et al. recommended that polymerization in water using a water-soluble RAFT agent could decrease chain transfer to the solvent. Still, no test results were provided to back up this claim [61]. During γ -irradiation, RAFT agent-mediated acrylic acid polymerizations in the aqueous solution and bulk were done independently [62]. UV light was also used to RAFT polymerize acrylic acid in the liquid media at room temperature. Nevertheless, an extra device is necessary for either γ -irradiation or UV-irradiation. The architectures of the RAFT compounds will have a significant impact on the live feature of polymerization in a common RAFT reaction [63,64]. The optimum choice for a RAFT agent is dithiocarbonate, whose intermediate radical is less stable than dithioester, according to studies on the polymerization of polar monomers and AA by RAFT [65]. Ji et al. reported a great structure of PAA with a molecular weight using RAFT synthesis in the aqueous phase is a logical option [66].

It is worth mentioning that PAA is similar to glass solids without color at ambient temperature, with the former having a glass conduction temperature of 106 °C and the latter having a glass transition temperature of 230 °C, which cannot be measured immediately due to its high temperature but can be inferred using copolymer statistics. It is soluble

in alcohols, methanamide or formamide, water and alkali water (pH of 8 or 9), and DMF. Theta solvents of PAA in which side chains react as perfect chains are 1,4-dioxane and 0.2 M aqueous hydrochloric acid [67,68]. It is also notable that theta solvents fall in between desirable and non-solvents. It is noteworthy to mention that theta solvents for poly (acrylic acid sodium) have been reported to be 1.5 M aqueous sodium bromide at 15 °C and 1.12 M aqueous sodium thiocyanate at 30 °C. Most PAA carboxyl groups do not react with water or 1,4-dioxane at neutral pH [69]. The chain design in 1,4-dioxane seems to be near the random coil because the main chain's C–C connections are very flexible at ambient temperature. Once PAA is neutralized by sodium hydroxide, the rate of separation improves. Practically all of the sodium acetate sites for NaPAA disintegrate in water. NaPAA acts like a traditional polyelectrolyte in aqueous, with n negative charges on each 0.25 nm of the polymeric chains. The solution viscosity is much greater than the random coil solution with the same amount and polymer chain length. The long-range electrostatic repulsive force between two anionic types substantially stretches the polymer chains. This suggests that high-molar-mass NaPAA and partially neutralized PAA can be used as a thickener. It is employed in poultices to maintain drugs on the skin surface [70]. Several different methods are employed to examine and characterize PAA. Some are used in other fields, such as infrared spectroscopy, gas and liquid chromatography, spectrometry, and nuclear magnetic resonance; in contrast, others are used mainly in the branch of polymers, such as osmometry size-exclusion, field-flow fractionation, and light scattering [71].

3. Architectures of PAA

3.1. Nanofibers

Nanofibers (NFs) have gained a particular interest owing to their unique physical and structural properties, i.e., large surface area, increased porosity, small pore size and fiber diameter, increased flexibility during functionalization of the surface [72]. Additionally, these possess high liquid or air permeability and rapid internal surfaces and form strong hydrogen bonds. Garza et al. [73] fabricated the nanofibers of PAA by subjecting the solutions of PAA for centrifugal spinning with various concentrations (9 to 14%) and speeds (4000 to 8000 \times g rpm), revealing different architectures of PAA nanofibers. When centrifuged at 6000 \times g rpm with 12 wt %. The average diameter of nanofibers was found 1100 nm when 12 wt % of PAA solution was placed for centrifugally spun at 6000 \times g rpm while the size was decreased to 900 nm in the case of 8000 rpm with the same concentration suggested the evaporation of the solvent in the fast spin rate resulting stretching of the nanofibers. The smallest diameter was found in the case of 9 wt %, which suggested that lower concentration led to smaller fiber average diameter, Figure 3a–c. PAA/PVA (in various molar ratios) electrospun nanofibers were stabilized by thermal crosslinking at 140 °C. The average diameter was found 309 ± 87 nm, 340 ± 83 nm, 290 ± 61 nm, and 221 ± 45 nm, for the molar ratios of 19.81, 35.65, 55.45 and 83.17, respectively for PAA/PVA [74]. This decrease resulted from the increment of conductivity and decrement of viscosity with increasing the PAA ratio. Eventually, the membranes maintained their fiber-based morphology joining at their points of contact after water immersion unveiled the porous architecture of PAA [75].

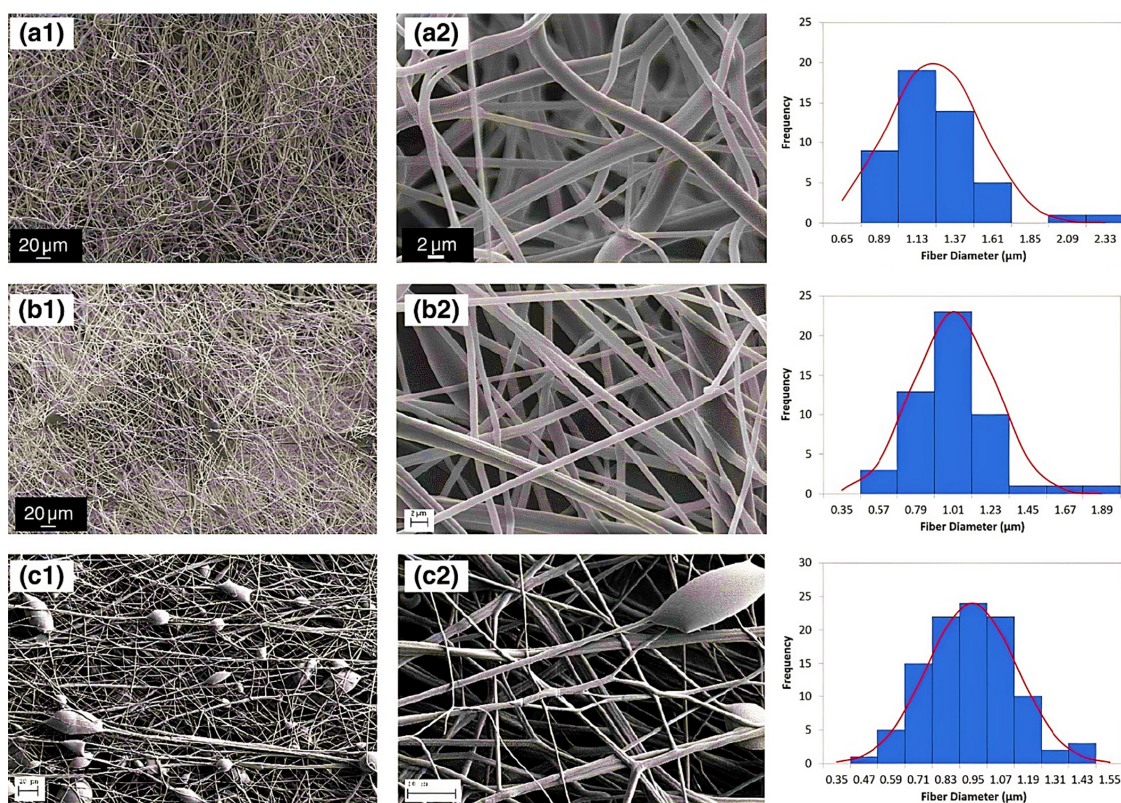


Figure 3. Diameter distribution and SEM micrographs of nanofibers of PAA (a) concentration of 12 wt% PAA and speed of 6000 rpm, (b) concentration of 12 wt% PAA concentration and speed of 8000 rpm, and (c) concentration of 9 wt% PAA concentration and speed of 4000 rpm. The SEM micrographs were taken at various magnifications: (a1,b1) 600×, (c1) 300×, (a2,b2) 7000×, and (c2) 15,000×. (Reprinted from Ref. [73] with permission).

3.2. Nanoparticles

Nanoparticles are materials with overall dimensions in the nanoscale, ie, under 200 nm. In recent years, these materials have emerged as important players in modern medicine, with clinical applications ranging from contrast agents in imaging to carriers for drug and gene delivery into tumors [76]. Nanoparticles of PAA have been extensively studied in biomedical applications such as drug delivery due to the unique capability to deliver drugs, genes, and proteins via the peroral route. The thiolated PAA nanoparticles were developed by Greindl et al. [77], whose architecture was covalently crosslinked via disulfide bonds. The cross-linkage of PAA with 2,2'-(ethylenedioxy)bis(ethylamine) (EDBEA) showed spherical morphology and 20–80 nm-sized nanoparticles [78], while the PAA-PS-Ag composite nanoparticles revealed spherical morphology with 3 ± 1.2 nm sized particles [79]. The exact morphology was obtained by Müller et al. [80] with a mean diameter <200 nm. The human fibrinogen binding kinetics depended on the size of negatively charged PAA/Au nanoparticles. The larger nanoparticles revealed binding with fibrinogen with a slower dissociation rate and increasing affinity. When the size of nanoparticles was 7 nm, the two nanoparticles were accommodated by each fibrinogen molecule, but when the size increased up to 10 nm, only one was adapted. The size increments up to 10–12 nm changes from one site to the two-site binding. The bound nanoparticles felt more coulombic repulsion when the diameter was increased. Due to the flexibility of both binding sites, one nanoparticle with a sufficient diameter (15–17 nm) was also found enough for the interaction of fibrinogen. Hence, more than 12 nm, multiple protein molecules were found, Figure 4i [81]. PAA-coated iron oxide nanoparticles showed two types of molar mass (1800 and 5000) due to the different architecture of PAA chains, which influenced the molar mass. The magnetic diameter of these nanoparticles was found in between 7.3 to 11.9 nm [82].

The architecture of nanoparticles of PAA-chitosan (CS) was dependent on the synthesis and pH of the synthetic medium. The nanoparticles at 4.5 pH (acetic buffer solution) revealed consistent and solid spherical particles unveiling PAA-CS nanoparticles' matrix structure. PH 7.4 showed a dense core bounded by a fuzzy and diffuse coating 4 (ii). This architecture was due to ionic interaction between negatively charged PAA and positively charged CS. The different preparation processes of PAA-CS nanoparticles influenced the architecture of nanoparticles. When PAA was dropped into a solution of CS, the generation of PAA core occurred, and a membrane was formed on the PAA core surface resulting in a dark shell and soft-core spherical nanoparticles. On the other hand, When the CS solution was dropped in the PAA solution, the core of CS and membrane of PAA-CS were formed. There were no cavities formed in PAA-CS because of the not swelling of CS in acidic medium, Figure 4iii. These all structures were created due to the construction of samples, conditions of staining, etc. [83]. The PAA magnetic nanoparticles possessed uniform particles morphology with a 9.2 ± 2.6 nm average diameter while a hydrodynamic diameter of 246 ± 11 nm ($n = 3$) was measured by the dynamic light scattering (DLS) measurements [84]. The other magnetic nanoparticles of PAA had a 10 nm size and were semispherical in shape [85]. PAA-coated iron oxide nanoparticles revealed a 10.1 ± 2.4 nm mean particle size. These were stable in water, and variation in pH or enhancement in ionic strength resulted in aggregation of these nanoparticles in water [86].

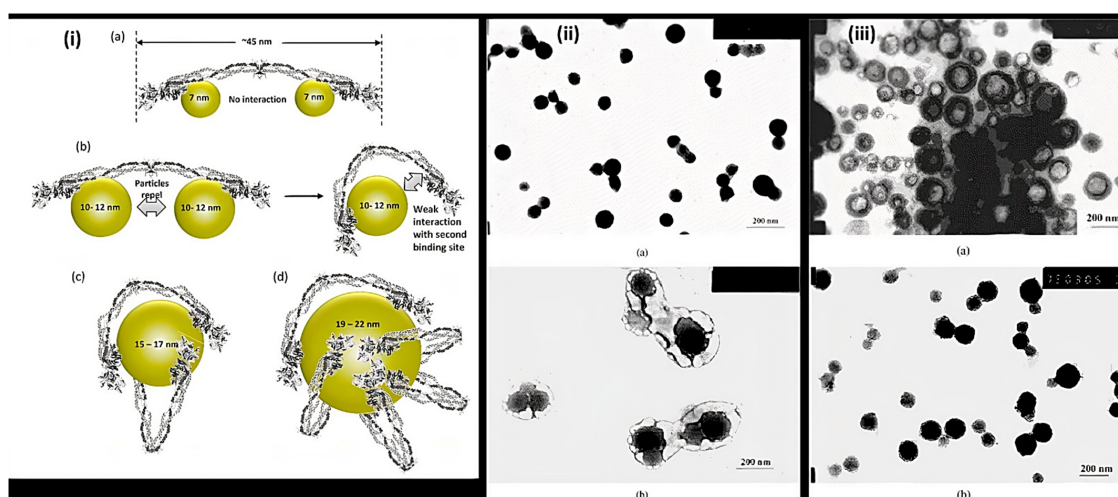


Figure 4. Representation of (i) binding of fibrinogen with PAA/Au nanoparticles (a) Binding of 7 nm nanoparticle to fibrinogen revealing each protein molecule accommodated two nanoparticles (b) 10–12 nm-sized nanoparticles prevent the binding of two particles to each fibrinogen due to the flexibility of fibrinogen at E domain of protein resulting the contact of second binding site with the nanoparticle (c,d) Larger nanoparticles (15–22 nm) can accommodate multiple fibrinogen molecules due to the larger surface area (ii) TEM of PAA-CS nanoparticles at (a) pH = 4.5 and (b) at pH = 7.4. (iii) Morphology of PAA-CS nanoparticles synthesized by the various processes at 4.5: (a) CS dropping into PAA solution; (b) PAA dropping into CS solution, (Reprinted from Refs. [81,83] with permission).

3.3. Nanocapsules

Nanocapsules have been the most extensively studied for functional compounds delivery [87]. Nanocapsule possesses a large inner cavity which helps in the high loading of drugs and sustained release of drugs due to its capsule-like structure [88]. The hollow tailor-made 100 nm nanocapsules of PAA/CS were fabricated for antibiotic therapy by Belbekhouche et al. [89]. Nanocapsules of PAA-N-isopropylacrylamide (PNIPAm) hydrogel are presented in Figure 5i suggests the polymerization and crosslinking of PAA with PNIPAm to form the nanocapsule architecture and unveiled the round shape morphology (135 nm) for PAA-hydroxypropylcellulose (HPC) template particles. At the same time, the

figure was seen in the 1st step above. After crosslinking with PNIPAm, the core (dark) shell (dusky) structure was seen, increasing the size to 230 nm. Even after removing the template, the particles maintained the spherical morphology with a larger inner cavity and thin shell having 50 ± 12.5 nm thickness, Figure 5ii [90]. The Nanosphere of PAA/BSA showed the 80 nm diameter while the nanocapsules revealed the 300–500 nm. These were synthesized using in situ polymerization, swelling, and re-aggregation. The interior diameter was found 100–200 nm, and glutaraldehyde (GA) cross-linked PAA/BSA nanospheres increased the stability. After absorbing the water molecules into PAA/BSA/GA also, nanocapsules were also formed. Microspheres presented the porous shape, and the hollows were small in nanocapsules that suggested that the architecture of PAA/BSA was fixed by cross-linking agents and reduced its flexibility, Figure 5iii [91]. Nanocapsules of PAA-*b*-PAN di-blocks were prepared using PAA macroinitiators using RAFT polymerization. The same architecture revealed monodisperse and spherical with 30–35 nm hydrodynamic diameter analyzed by dynamic light scattering and TEM. The aggregation of these nanocapsules was occurred by π - π interaction of the graphite layers [92]. In situ acrylic acid polymerization was done to obtain liposome nanocapsules coated with PAA with a mean diameter of 123 ± 21 nm [93]. The core-shell structure for copolymers of PAA was seen in the nanocapsules of PAA with an average diameter of 70 nm and 10 nm of shell thickness [94].

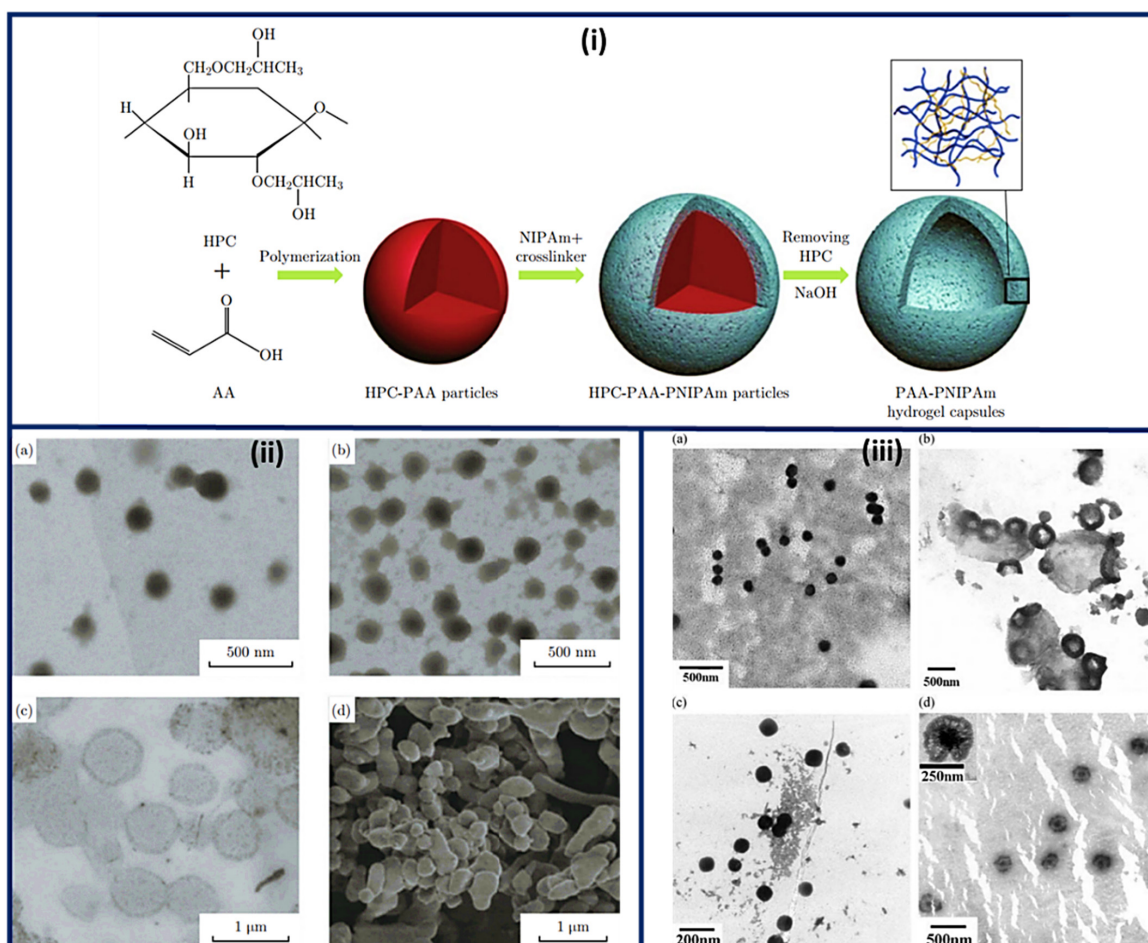


Figure 5. Schematic representation of the (i) synthesis and architecture of PNIPAm-PAA hydrogel capsules (ii) TEM micrographs of (a) PAA-HPC particles (pH 2.4) (b) PNIPAm-PAA-HPC composites (pH 2.4), (c) PNIPAm-PAA hydrogel capsules (pH 8.0) and (d) SEM image of PNIPAm-PAA hydrogel capsules after freeze-drying procedure. (iii) Morphology of nanosphere and nanocapsule of PAA/BSA (a) PAA/BSA, (b) nanocapsule of PAA/BSA, (c) PAA/BSA/GA, and (d) nanocapsule of PAA/BSA/GA. (Reprinted from Refs. [90,91] with permission).

3.4. Other Structures

Poly (acrylic acid-*b*-isoprene) cross-linked micelle structures were synthesized using calcium phosphate coating (20 nm thickness) having 60 ± 9 nm mean diameter, revealing the mineralization near or at surface regions of PAA. Additionally, nanocages were also formed. These hybrid materials were found stable for numerous months in water. Even though it aggregated and mineralized with time, there was no change seen in crystallization and diameter even after eight months (Figure 6a,b) [95]. Spherical microspheres of PAA/PVA of sequential interpenetrating network crosslinked with GA were obtained via SEM analysis. Figure 6c suggested spherical morphology without any agglomerations. A smooth microspheres surface was obtained with no pores, and some particles were covered with polymeric debris, Figure 6d [96]

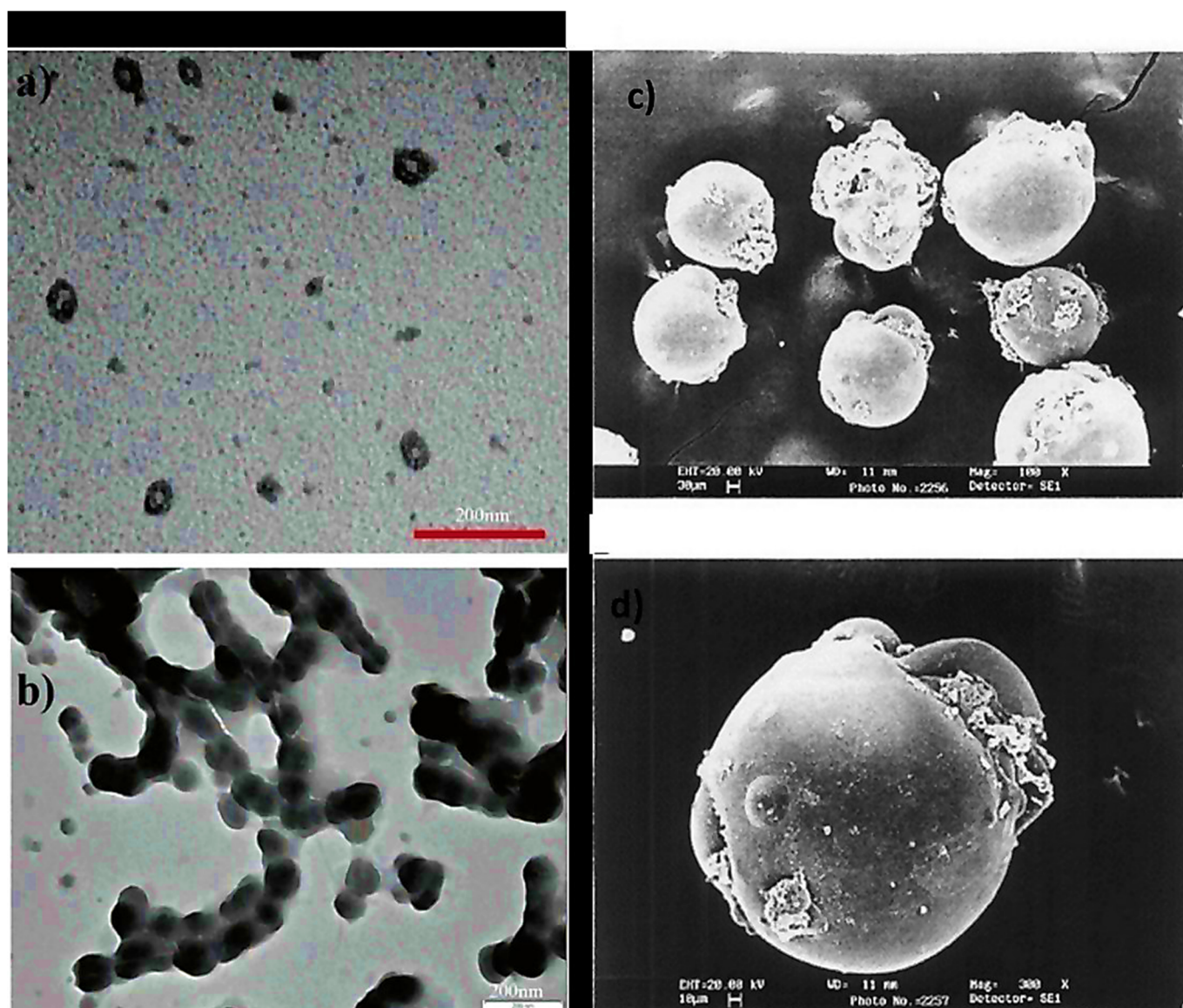


Figure 6. TEM micrographs of (a) cross-linked PAA-*b*-PI micelles covered with calcium phosphate, (b) PAA nanocages-Calcium phosphate displaying enhanced levels of aggregation and mineralization (after eight months) (c) SEM microspheres of PAA without forming agglomerations (spherical) (d) The smooth surface of microspheres without any pores. (Reprinted from Refs. [95,96] with permission).

4. Bio-Conjugation with Other Materials

Surface modification has been considered an effective method of improving material performance, modulating their properties, and extending their applications [97]. The layer-by-layer assembly deposits many coating layers on the surface, and self-assembled monolayers need a match between surface and sorbate chemistry are the two dominant strategies in surface modification chemistry. After that, the coating polymers are considered a surface modification for various applications. Among these polymers, PAA, because of its outstanding surface adherent properties, induces functional groups and biocompatibility and has been extensively used as the coating agent [98]. Various surfaces containing metal oxides, gold nanoparticles, metal-organic framework, silica, and carbon-based materials (carbon nanotubes, graphene) were coated using this polymer. The PAA films coated onto the surface of nanomaterials can improve their stability and solubility and facilitate functionalization of them to make intelligent materials. PAA film may theoretically add anticancer medicines and contrast agents to the surfaces.

4.1. Metal Oxides

Fe_3O_4 nanoparticles (NPs) are many metal oxides widely used as coating agents on surfaces. The PAA-coated Fe_3O_4 NPs have an inherent magnetic feature that allows them to be collected using an external magnetic field [99]. These nanomaterials have magnetically assisted therapies, and MRI uses in nanomedicine. Yunn-Hwa Ma et al. used a coprecipitation approach to make Fe_3O_4 NPs, which they subsequently modified with a PAA film and recombinant tissue plasminogen activator (rtPA). The Fe_3O_4 @PAA NPs were used for the targeted delivery of rtPA by using an external magnetic field. The findings demonstrated that using a magnetic field could improve nanoparticle accumulation in tumor tissue [100]. Diana Couth et al. constructed Fe_3O_4 @PAA NPs ranging from 8–11 nm in a separate study. The in-vitro effect of Fe_3O_4 NPs coated with PAA and bare was evaluated on the induction of six cytokines. The findings displayed that both polymer-coated and bare NPs could induce all of the cytokines examined [101].

Shuo-Li Sun et al. synthesized Fe_3O_4 NPs coated with PAA and then imbedded with polyethylenimine. At the end of production, the fabricated system was used for delivering plasmid DNA by using an external magnetic field. The results demonstrated that magnetoreception efficiency in HEK 293T and U87 cells increased in an external magnetic field [102].

A new aluminum hydroxide nanostructures embedded with PAA coated Fe_3O_4 NPs were developed and studied as dual MRI/positron emission tomography (PET) contrast agents for cell imaging by Manuel Antonio González-Gómez et al. [103].

Zhaoqiang Zhang et al. synthesized a biocompatible and superparamagnetic hollow mesoporous nanoparticle based on Fe_3O_4 NPs with the ability of magnetic targeting. Then the nanoparticles were coated with PAA, which can load bleomycin (BLM) through bonding with PAA in the mesoporous structure (Figure 7A–C). The results demonstrated that designed systems could effectively load drug and release it sustainably. The therapeutic efficacy of hollow magnetic NPs was much higher than free drugs [104].

Daniela Rodrigues et al. studied in-vivo biodistribution of PAA coated Fe_3O_4 NPs. In their study, after 24 h of intravenous administration of NPs, the expression of iron in mouse liver and spleen tissues was measured using histochemistry. According to the findings, iron deposition was found in macrophages from both organs [105].

Arkaban et al. designed a theranostic system based on CoFe_2O_4 coated with PAA and conjugated with folic acid (FOA) and doxorubicin (Dox) for theranostic intentions. This combination displayed increased diagnostic and therapeutic efficiency [106]. The theranostic system showed a size around 43 nm in diameter, while the thickness of PAA layers was about 12 nm. Finally, the theranostic system was used to treat cancer breast cells based on its chemotherapy influence; compared to non-targeting systems and free Dox, this method has better chemotherapeutic properties.

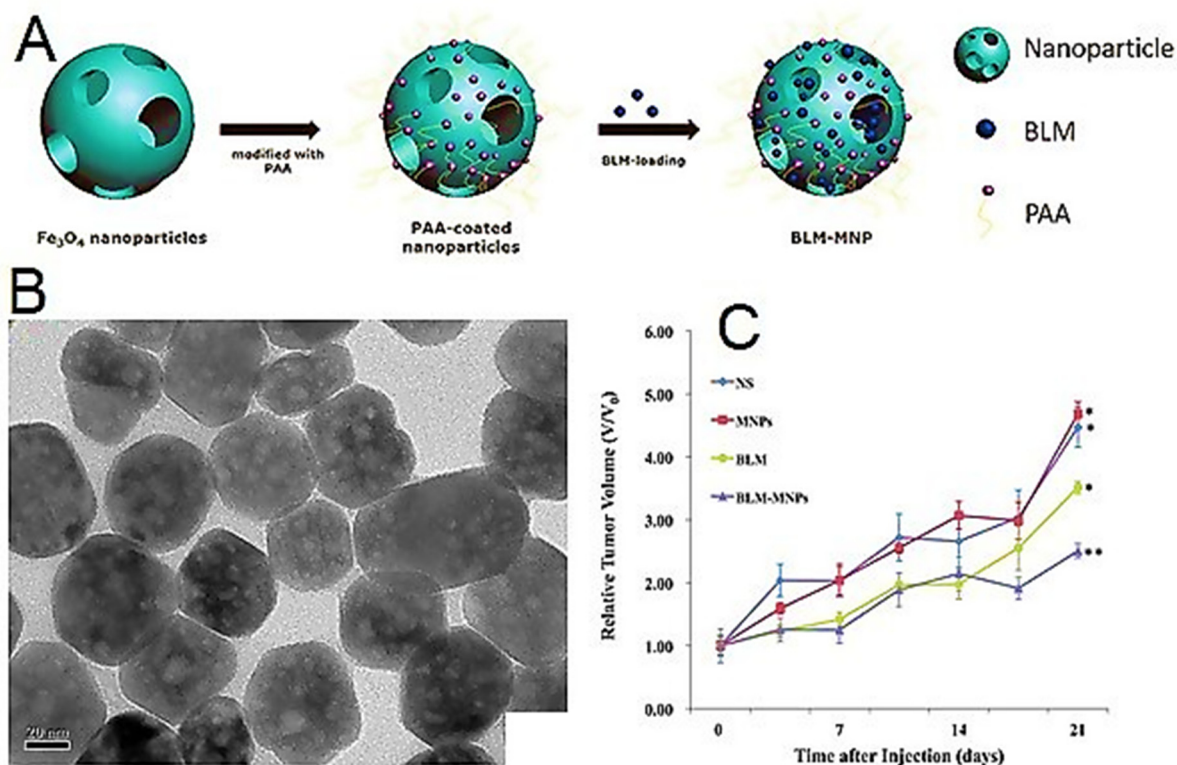


Figure 7. (A) Step-by-step synthesis of magnetic nanoparticles with PAA coating in the outer layer and BLM molecules adorned with PAA is depicted in this figure. (B) TEM image of bare nanoparticles. (C) The therapeutic effect of BLM-MNPs on tumors under the magnetic field. After several treatments, the relative tumor volume of several groups of mice showed ($n = 6$): mice injected with NS, MNPs, BLM, and BLM-MNPs [104].

Other metal oxides were also covered with PAA to create usable nanoplateforms. T1-weighted MRI agents such as Mn oxides can be employed for imaging-guided therapy. Marzieh Samiei Foroushani et al. presented a multifunctional theranostic structure constructed of manganese oxide (Mn_3O_4) NPs, covered with PAA, and loaded with methotrexate targeting agent and anticancer drug. PAA, a pH-sensitive agent for loading and delivery of MTX, can improve MTX accumulation in tumor sites [107].

Arkaban et al. fabricated a nanocomposite system, including Au NPs, coated sequentially by $\text{MnCO}_3/\text{Mn}_3\text{O}_4$ and PAA. Then, the PAA-immobilized NPs were imbedded with FOA (as targeting agent), Dox (anticancer drug), and propidium iodide (fluorescence imaging agent). The fabricated nanosystem displayed good encapsulated drug and encapsulating efficiency and increased ability for catching of 4T1 cancer cells when compared with non-targeted system and free Dox [108].

The manganese dioxide nanoparticles (MnO_2) coated with PAA were synthesized. Their influence on lung cancer cells with or without gefitinib was reported by Me Hyeon Cho et al. In MR imaging, MnO_2 NPs exhibited glutathione (GSH)-responsive dissolution and subsequent enhancement. Moreover, the therapeutic data demonstrated upon using X-ray irradiation, the therapeutic efficiency of MnO_2 on lung cancer cells was considerably enhanced [109].

Khan et al. discussed the possible interactions between materials such as poly(xyloglucan-co-methacrylic acid), hydroxyapatite, and silica [110]. Figure 8 depicts a possible interaction between metal oxide and PAA.

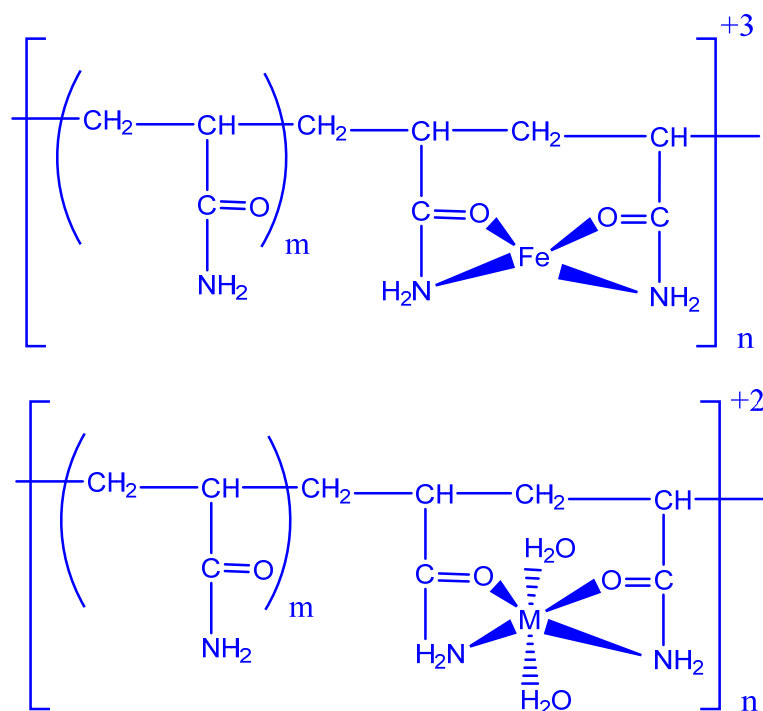


Figure 8. The proposed interaction between PAA and metal.

4.2. Gold Nanostructures

Gold nanostructures have been considered in various fields because of their excellent physicochemical features, such as nontoxicity, suitable biocompatibility, simple methods for preparation, and excellent optical properties. Different gold structures have been fabricated, containing nanospheres, nanoclusters, and nanorods. The surface modification of gold nanomaterials with PAA for nanomedical applications is the focus of this paper.

Su Pan et al. synthesized PAA-coated gold nanorods (GNR@PAA). First, Cetyltrimethylammonium bromide-coated gold nanorods were synthesized by a seed-mediated procedure. Second, the nanorods were further coated with a PAA film. Finally, they discovered that hyperthermia therapy was more effective when GNRs@PAA was combined with a laser. They investigated the process of GNRs@PAA radiation treatments. They found that disrupted cell membranes and DNA integration cause cell apoptosis and death, with the cell apoptosis rate boosted by *in vitro* photothermal therapy [111].

In a separate Guilan Li et al. studied a standard method for fabricating gold nanorod@polyacrylic acid/calcium phosphate (AuNR@-PAA/CaP) core-shell NPs containing PAA/CaP shell and an Au rod as the core. They showed that AuNR@PAA/CaP core-shell NPs had a high drug encapsulating ability (1 mg Dox/mg NPs), excellent photothermal feature (26%), and pH/near-infrared dual-sensitive behavior. Because the CaP shell is destroyed at low pH values, releasing Dox increases. NIR irradiation of the Dox loaded in the AuNR@PAA/CaP core-shell NPs was released. AuNR@PAA/CaP core-shell NPs have also been effectively used in synergistically dual mode X-ray computed tomography/photoacoustic imaging as well as chemo-photothermal cancer treatment [112].

Gold nanostars (GNs) were coated using PAA sheets in addition to nanorods to create usable nanoplatforms. Spherical gold nanocrystals covered with PAA/mesoporous silica shell NPs (AuNC@PAA/mSiO₂ NPs) with having accumulation enhanced fluorescence (AIF) properties were described by Xiaotong Wu et al. The manufactured NPs have been used as therapeutic and diagnostic agents for liver cancer chemo-therapy and synergistic fluorescence/X-ray computed tomography imaging. Surprisingly, the produced NPs had many AIF characteristics (equivalent to 4.2 times the individual AuNCs) and high drug loading and pH-responsive drug release [113].

Chixia Tian et al. described an MRI/CT bimodal imaging agent constructed of Gd-MOF and gold nanoparticles (AuNPs). PAA was employed to bridge Gd-MOF NPs and AuNPs, fabricating hybrid Gd-MOF/AuNPs. The obtained hybrid NPs were then estimated in dual imaging (MRI and CT). The findings demonstrated great relativity in MRI and CT imaging [114].

Gold nanoparticles can be integrated with PAA for several applications. Rezvani et al. created various core-shell NPs with AuNPs as the core and stimuli-sensitive polymers such as PAA, poly(N,N methylene bis(acrylamide))(PMBA), poly(methacrylic acid) (PMAA), poly(2-hydroxyethylmethacrylate)(PHEMA), and poly(N-isopropylacrylamide) (PNIPAAm), as shell [115]. According to TEM pictures, all core-shell NPs were smaller than 100 nm. The loading efficiency of systems was studied. Researchers observed that Au-PMAA and Au-PAA NPs had a high amount of drug loading because of effective interaction between the carboxyl groups of Dox and polymer. In addition, drug release was significantly increased under NIR light.

Zhou J. Deng et al. were synthesized Au NPs coated with PAA with sizes 7–22 nm and examined their interactions with fibrinogen protein. They monitored the binding kinetics of human fibrinogen to negative PAA-coated Au NPs and understood that the bigger NPs bound fibrinogen with high attraction and a gentler disconnection rate. While each fibrinogen molecule could collect two 7 nm NPs, only one fibrinogen molecule could aggregate 7 nm NPs. Several fibrinogen molecules were connected by NPs bigger than 12 nm. In any case, fibrinogen produced aggregation of the larger particles in the presence of additional NPs, which might connect more than one protein particle. This is comparable with fibrinogen interparticle bridging. Overall, the findings indicate that appropriate modifications in NP size can alter protein binding both on the NPs' surface and within the protein corona [81].

Chunyuan Song et al. designed a nanocarrier with excellent loading efficiency and pH-responsive release behavior based on a flower-like Au NPs. The surface-enhanced Raman scattering active floral nanoparticles with a high surface area were synthesized and subsequently modified with thiolated-PAA (PAA-SH) for efficient pH-dependent loading and release of Dox as an anti-cancer medication [116].

4.3. Silica Nanoparticles

Lu Li et al. suggested a synthetic method for the fabrication of $\text{Fe}_3\text{O}_4@m\text{SiO}_2@PAA$ nanoclusters (NCs) and studied their applications in MRI and as a pH-sensitive DDS. First, they converted the oleic acid-capped Fe_3O_4 NPs to Fe_3O_4 coated with CTAB and then the formed fluorescein isothiocyanate (FITC)-labeled fluorescent $m\text{SiO}_2$ shells on CTAB- Fe_3O_4 NPs. Then, the -synthesized $\text{Fe}_3\text{O}_4@m\text{SiO}_2$ NPs modified with the PAA shells. Finally, the obtained NCs were applied as DDS and fluorescent labels for imaging and therapy intentions. The results revealed that the fabricated system could load a lot of drugs and release them in a pH-dependent manner. Moreover, in-vitro tests verified that the NCs are biocompatible, and the Dox-loaded NCs had a high cytotoxic effect on cancer cells [117]. Also, Zhen Xia et al. designed a DDS constructed of $\text{CaF}_2:\text{Yb,Er}$ NPs coated with SiO_2 nanofibers ($\text{CaF}_2:\text{Yb,Er}@m\text{SiO}_2$) for Dox delivery. The results showed importing PAA on silica nanofiber can improve the loading ability of the fiber. Also, PAA-coated $\text{CaF}_2:\text{Yb,Er}@m\text{SiO}_2$ nanofibers revealed light and pH-dependent release. Dox release rate and in-vitro anti-cancer efficacy were improved by irradiation with a NIR (808 nm) laser [118].

4.4. Metal-Organic Frameworks (MOFs)

MOFs fabricated of metal ions and organic linkers. These porous crystalline materials are used in various fields because of having an excellent surface area, stability, porosity, and biocompatibility [119]. MOFs are frequently utilized as nanocarriers because of having good loading efficacy and sustained drug release properties [120].

Tran et al. constructed a nanostructure based on ZIF8 with high encapsulation ability for Dox delivery (Dox-loaded ZIF8). The Dox-loaded ZIF8 was modified with PAA (ZIF8-

Dox@PAA) (Figure 9). Finally, they have studied the release manner of Dox at different pH and the influence of various factors on its release [121].

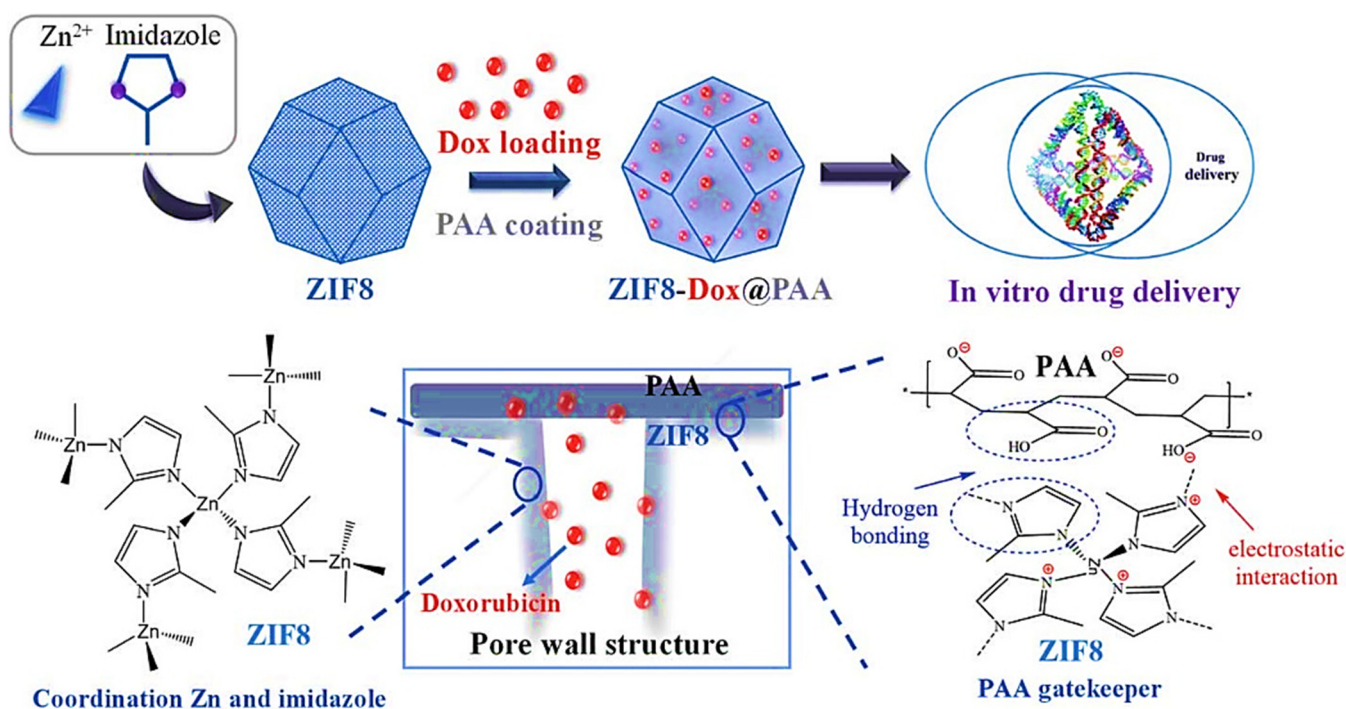


Figure 9. The preparation of ZIF8–Dox@PAA is depicted schematically [122].

In another study, Amin Bazzazadeh et al. fabricated the magnetic MIL-53 particles coated with PAA grafted-chitosan/polyurethane core-shell NPs for delivery of temozolomide (TMZ) and paclitaxel (PTX) toward U-87 MG glioblastoma cells [120].

4.5. Carbon Nanomaterials

Ming Xu et al. determined the toxicity effect of GO. They found from in-vitro experiments that pristine GO could hurt cell functions and cell membrane integrity. To increase the biocompatibility of GO, they were modified with poly(acrylamide), poly(ethylene glycol), and PAA. GO coated with PAA revealed the most biocompatibility [40].

The multi-walled carbon nanotubes (MWCNT) combined with iron oxide NPs because of their unique properties (nontoxicity, magnetic features) have been considered drug carriers. The low circulation time in biological fluids is one of the most significant drawbacks of these NPs. To overcome this problem, Bardajee et al. coated MWCNT with PAA and swelling kinetics and their capability to load and release tetracycline hydrochloride in various conditions studied [122].

Yunping Chen et al. synthesized graphene nanosheets (GNSs) by direct current arc discharge and functionalized and loaded them with hydrophilic PAA and Dox, respectively (GNSs-PAA(Dox)_{load}). Results showed that PAA(10 wt%)-GNSs significantly improve the solubility of GNSs in aqueous solution and have a high loading efficiency of 2.404 mg/mg at the concentration of 0.36 mg/mL of Dox. Also, the PPA-GNSs showed acceptable pH-sensitivity [123].

At two distinct pH values, C. Sgarlata et al. investigated the physisorption process, and hydration behavior of gemcitabine (GEM) PAA GO. The energy of physisorption and the hydration shell around the complex is affected by the varied ionization of pH-sensitive groups. A decrease aids the physisorption process between PAA and GO in negative charge density, occurring at acidic pH. However, a modest interaction between GEM and PAA is found at the same pH setting. Compared to unionized GO and bulk water, the radial distribution function (RDF) shows that carboxylate oxygens of PAA and alkoxide oxygens

of GO significantly attracted dipolar water molecules, affecting the hydration shell around the complex [124].

4.6. Other Metals

Adibehalsadat Ghazanfari et al. prepared five types of PAA-covered small metal oxide NPs with an average size of 2.3, 1.7, 1.5, 1.8, and 1.9 nm, respectively (Bi_2O_3 , Yb_2O_3 , NaTaO_3 , Dy_2O_3 , and Gd_2O_3) and characterized their X-ray attenuation features, and accomplished in-vivo CT imaging using of the samples. Results showed that all NPs have outstanding colloidal stability and biocompatibility, and X-ray attenuation powers are more significant than those obtained for commercial iodine contrast. They extracted X-ray attenuation efficacies 11.7, 6.8, 10.3, 6.1, and 5.9 HU/mM for PAA-coated ultrasmall Bi_2O_3 , Yb_2O_3 , NaTaO_3 , Dy_2O_3 , and Gd_2O_3 NPs, respectively. Also, they investigated the NPs as CT contrast agents in CT images in the mouse organs [125].

Xuekun Jia et al. successfully synthesized PAA-modified $\text{NaYF}_4:\text{Yb}$, Er NPs (PAA-UCNPs) with the dual drug carrier and imaging capabilities. They used the PAA as a pH-responsive system to encapsulate drugs via electrostatic interaction. The drug encapsulation efficacy of the PAA-UCNPs was examined using Dox to assess their potential as a nanocarrier system. The loading and release of Dox loaded on PAA-UCNPs depended on varying pH. While a low amount of Dox was released at a weak alkaline medium, an increased release was observed in an acidic medium. The in vitro cytotoxicity test indicated that the PAA-UCNPs loaded with Dox were cytotoxic to HeLa cells [126].

Yufei Ma et al. produced and employed $\text{NaYF}_4:\text{Yb}^{3+}, \text{Er}^{3+}$ NPs (UCNPs) to monitor rabbits' bone tissue mesenchymal cells (MSCs). To increase biocompatibility and cellular uptake of NPs, they coated the UCNPs with a negative polymer PAA and a favorable poly(allylamine hydrochloride) (PAH-PAA-UCNPs). In terms of ALP activity, osteogenic protein expressions, cell viability, and the generation of mineralized nodules, no significant difference was identified between UCNPs-free MSCs and MSCs labeled with UCNPs (concentration range of 0–50 g/mL) (concentration range of 0–50 g/mL) [127].

Yan Ma et al. produced $\text{Co}_{0.85}\text{Se}$ NPs (PAA- $\text{Co}_{0.85}\text{Se}$ NPs) using an ambient aqueous precipitating technique for dual photothermal-chemotherapy of malignancies. PAA $\text{Co}_{0.85}\text{Se}$ NPs with outstanding photothermal conversion efficiency (45.2%), low cytotoxicity, significant near-infrared (NIR) light absorption, and ultrasmall size (8.2 nm) were produced. Dox encapsulated on PAA- $\text{Co}_{0.85}\text{Se}$ NPs with a loading efficiency of 8.3%, which showed a pH-sensitive release behavior because of the protonation of carboxyl groups in PAA molecules and amino groups in Dox. Also, they studied the cytotoxic effect of PAA- $\text{Co}_{0.85}\text{Se}$ -Dox NPs on HeLa cells. Irradiation with a near-infrared laser had a significant synergistic cell killing impact and increased treatment efficacy [128].

Hanzhu Shi et al. synthesized PAA/ CaCO_3 NPs using a primary and new procedure. PAA/ CaCO_3 NPs were not only substantially more effective at loading Dox (1.18 g of Dox per g of NPs), but they also had a pH-sensitive characteristic. In vivo tests revealed that Dox-loaded PAA/ CaCO_3 NPs have a considerable anticancer impact with no noticeable adverse effects [129].

Kai Zhang et al. designed a drug carrier based on PAA-adorned three-dimensional (3D) MoS_2 NPs (PAA- MoS_2 NPs) that respond to NIR laser irradiation for the treatment of hypertension utilizing atenolol (ATE). The drug encapsulation efficacy and photothermal converting effect of PAA-coated MoS_2 NPs were also investigated. The PAA- MoS_2 NPs had a high drug-loading ability of 54.99 percent and a high photothermal efficiency. Further, they have explored the controlled release capacity of the PAA- MoS_2 NPs using in-vitro drug release and skin-penetration studies. In the laser-stimulated group, drug release was 44.72 percent, and skin permeability was improved by a factor of 1.85 [130]. PAA-based core-shell nanostructures on various substrates are summarized in Table 1.

Table 1. PAA-based core-shell nanostructures on a variety of substrates.

Substrates	Substrate Form	Refs.
Fe ₃ O ₄	nanoparticles	[131–139]
Fe ₃ O ₄	nanogels	[140]
Fe ₃ O ₄	ferrogels	[141]
Fe ₃ O ₄	hydrogel	[142]
γ-Fe ₂ O ₃	nanoparticles	[143]
CoFe ₂ O ₄	nanoparticles	[144,145]
NiFe ₂ O ₄	nanoparticles	[146]
Multi-walled carbon nanotubes	nanocomposite	[122]
Mn ₃ O ₄	nanoparticles	[147]
MnCO ₃	microcapsules	[148]
Co ₉ S ₈ @MnO ₂	nanoparticles	[149]
Fe ₃ O ₄ @MnO ₂	nanoparticles	[150]
Fe ₃ O ₄ @MnO ₂ -doped NaYF ₄ :Yb/Er/Nd	nanosheets	[151]
Au NPs	nanoparticles	[152–155]
Au NPs	hydrogel	[156]
Au NPs	nanoclusters	[157]
Au NPs	nanorods	[158]
SiO ₂	nanoparticles	[159–163]
Au NPs@SiO ₂	rubber film	[164]
MOF	nanoparticles	[165]
rGO	hydrogel	[166]
Mg-Ca ₃ (PO ₄) ₂	clusters	[167]
TiO ₂	nanoparticles	[168,169]
CaCO ₃	nanoparticles	[170]
CeO ₂	nanoparticles	[171]

5. Biomedical Applications

Nanotechnology is the manipulation of matter on a near-atomic scale to produce new structures, materials and devices. The technology promises scientific advancement in many sectors such as medicine, consumer products, energy, materials and manufacturing [172–175]. New developments in science, bioinformatics and nanotechnology have significant impact on human health and life [176–179]. For example, bioinformatics is interdisciplinary fields, which harnesses computer science, mathematics, physics, and biology [180–183]. In other hand, PAA is employed in adhesives, coatings, homes, packaging, pharmacology, and other medical and biological industries [25].

5.1. Bio-Sensing

Hydrogels with excellent mechanical strength, rapid recovery, and shape memory capabilities based on PAA could open up new possibilities for various biomedical applications [184]. Carboxymethyl xylan-g-poly(acrylic acid) was designed to have strong compression strength, elongation, and elasticity, as well as shape memory capabilities activated by Fe³⁺ [185].

Endotoxins, commonly known as lipopolysaccharides (LPS), are infections produced from gram-negative bacteria's outer membrane and cause serious harm to humans. LPS detection that is sensitive and selective is in high demand, notably in medical supplies, pharmaceuticals, and food. MoS₂-PAA nanocomposite loaded with Au NPs was fabricated for the detection of LPS. Firstly, MoS₂ nanosheets were prepared using sonication-assisted exfoliation of bulk MoS₂ with PAA, and then it was immobilized using thiol terminated LPS binding aptamers, which were combined with Au nanoparticles [186].

The plasma polymerization approach was utilized to prepare electrode material consisting of hollow TiO₂ spheres and PAA for detecting lysozyme. According to electrochemical impedance spectroscopy data, the produced TiO₂ at PAA aptasensor has a very

sensitive detection ability toward lysozyme; the proposed aptasensor has a detection limit of 0.015 ng mL^{-1} in the range of $0.05\text{--}100 \text{ ng mL}^{-1}$. The film showed good selectivity for lysozyme in the medium containing interfering proteins such as immunoglobulin E, bovine serum albumin, and thrombin [187].

Nanospheres as immunoprobes were produced using chitosan-poly(acrylic acid) nanospheres doped with copper, cadmium, lead, and zinc ions to detect electrochemical signals and react with glutaraldehyde to immobilize various tagged antibodies [188]. Hydrogen peroxide with an excellent detection limit of $0.5 \text{ }\mu\text{M}$ using Met-hemoglobin was developed as an electrochemical biosensor [189].

Microgels' visible color and distinctive spectral features based on poly (acrylic acid-co-N-isopropylacrylamide) microgel-based have been demonstrated, and both depend on solution temperature and pH. Its sensitivity will be further exploited [190].

PAA brushes having carboxyl groups should be adaptable enough to allow for a wide range of chemical modifications, including the attachment of bioactive species that can be used as biosensor detecting probes. According to this research, PAA brushes with a predetermined graft density have shown to be a suitable precursor layer for biosensing applications [191].

Moreover, poly(tert-butyl acrylate) brushes were synthesized using the polymerization of tert-butyl acrylate. The tert-butyl groups from the poly(tert-butyl acrylate) bushes were removed by acid hydrolysis, yielding PAA brushes. The PAA brushes' carboxyl group density can be adjusted based on chain length or molecular weight. The carboxyl groups of PAA brushes were tested to immobilize biotin [192].

Functionalized polymer based on polystyrene core and PAA shell nanospheres with cadmium ions was used to detect human IgG. The carboxyl groups of PAA shells were used to chelate cadmium ions and then conjugate them with antibody (Ab2) to generate metal ions labeled bioconjugates that were used as the label in immunoassays. In the future, this method is projected to be used extensively in protein diagnostics and bioanalysis [193].

PAA- multiwalled carbon nanotubes are a hydrophilic composite poly(acrylic acid)-a wrapped complex demonstrating remarkable stability in basic and acidic pH conditions. The complex also shows strong resistance to moderate ionic strengths [194].

5.2. Bio-Imaging

Bioimaging is a critical diagnostic technique for studying and visualizing biological events in cells and medicine [195]. Chen et al. proposed a simple production approach for synthesizing nanoparticles based on PAA using atom transfer radical polymerization (ATRP). When activated by a 980 nm near-infrared laser, the nanoparticles disperse efficiently in water and emit a strong green light, indicating that they could be helpful for luminous bioimaging [196].

Uniform Nd^{3+} -doped LuVO_4 nanophosphors were produced and surface-coated with PAA; these nanoparticles are in a colloidal range in physiological pH range and have excellent stability to survive in the cell. Because of these features, these may be used as a bimodal probe for X-ray computed tomography and NIR luminous bioimaging [197]. CdSe/Cu quantum dot conjugates with biocompatible polyacrylic acid functionalization were produced for bio labeling, bioimaging, and biomolecule detection applications [198].

Polycrystalline and crystallized into a hexagonal shape of PAA-Eu-NaGdF₄ nanospheres were fabricated by Nunez et al. Their size could be changed in the 60–95 nm range, varying the amount of PAA applied. When activated with UV light, these nanoparticles showed red luminescence, and the smaller nanospheres showed tremendous promise to MRI [199].

To functionalize Bi- and Eu-doped NPs based on rare earth vanadates (MVO_4 , $\text{M} = \text{Gd}, \text{Y}$), poly(allylamine hydrochloride) and PAA were used. The cytotoxicity, colloidal stability in various biologically relevant buffer media, absorption by HeLa cells, and low pH degradability also proved suitable for bioimaging and biosensing applications [200].

Optical bioimaging has emerged as a vital technique for detecting diseases with great sensitivity. NaYF₄:Gd/Yb/Er nanorods modified by PAA were fabricated by Xue et al.

with increased NIR IIb emission for bioimaging applications. Without a craniotomy, non-invasive optical brain vascular bioimaging with excellent spatial (43.65 μm) and temporal resolution is acquired through the scalp and skull [201]. NaLuF₄: Gd/Nd nanorods modified by PAA were studied for high sensitivity *in vivo* optical imaging and NIR-II bioimaging-guided small tumor diagnosis. The NIR-II emission of the NaLuF₄: Gd host can be easily changed by doping Nd³⁺, resulting in a potential emission with strong photo-stability centered at 1056 nm and 1328 nm [202].

5.3. Cancer Therapy

New developments in science, bioinformatics and nanotechnology have significant impact on human health and life [203–207]. Cancer is a group of diseases involving abnormal cell growth with the potential to invade or spread to other parts of the body [208–213]. In this light, a hybrid material based on PAA and mesoporous silica nanoparticles was used for drug delivery systems in various ways, including surface modification, doxorubicin hydrochloride loading, and PAA coating. Doxorubicin was used as a model guest molecule to study drug encapsulation and release behavior at various temperatures and pH levels. It has the advantages of being easy to make, having no cytotoxicity, and having a high drug loading capacity, all of which could be useful in anticancer therapy [214]. A nanosized polyacrylic acid-polyaniline copolymer with increased water solubility was developed and proved to be an excellent option for wound healing and cancer therapy, particularly in the treatment of HT29 [215].

By using norepinephrine-loaded PAA nanogels as angiotonics, Li et al. have developed an anticancer auxiliary delivery method. The auxiliary system significantly reduced nano-drug uptake in the liver by raising the liver blood flow rate. The blood perfusion quantity rose dramatically by about 200 percent after administration of the as-prepared norepinephrine-loaded PAA nanogels, as measured directly by ultrasonic imaging, showing a higher blood flow rate in the liver [216]. For paclitaxel targeted delivery and anticancer efficacy, Reddy et al. designed sodium alginate grafted poly (acrylic acid-co-acrylamide/cloisite-30B/silver nanoparticle hydrogel composites with different weight percentages of cloisite-30B clay [217].

Erlotinib (ETB) is a commonly prescribed medication for non-small-cell lung tumors. To severe toxicity in clinical applications and avoid drug resistance, pH-sensitive and redox-responsive nanocarriers were developed to encapsulate ETB. Poly (acrylic acid)-cystamine-oleic acid was produced by emulsification followed by solvent extraction and converted into ETB-loaded lipid nanoparticles for lung cancer treatment [218].

Based on the bionics concept, Stimuli-responsive polymer materials are a new class of intelligent materials that exhibit more significant changes in physicochemical properties when activated by small environmental stimuli, making them an excellent carrier platform for anticancer medication delivery. Hybrid block copolymers based PAA, poly(2-methacryloyloxyethyl ferrocenecarboxylate), and Fe₃O₄ with dual stimuli responsiveness were developed using a two-step sequential reversible addition-fragmentation chain transfer polymerization process. It was non-toxic, stable, and entrapped hydrophobic anticancer drugs, which were then delivered quickly in particular microenvironments, including acidic pH and high reactive oxygen species [219].

Because it improves efficacy while reducing adverse effects, oral chemotherapy is the preferred method for cancer treatment. Unfortunately, the oral bioavailability of most anticancer medicines was inadequate. Tian et al. reported a pH-triggered oral medication delivery system using a simple graft-onto technique to cap mesoporous silica SBA-15 with pH-responsive PAA. PAA-capped mesoporous SBA-15 had a high drug loading capacity (785.7 mg/g), was pH sensitive, and had good biocompatibility. This pH-activated oral drug delivery device could be helpful in the treatment of colon cancer and other disorders [220].

Using a graft-onto approach, a nano-carrier based on PAA as shell and mesoporous hydroxyapatite nanoparticles as the core was developed, with an anti-proliferative effect on cancer cells. By electrostatic interactions, the grafted PAA may significantly enhance the

loading quantity of the medication doxorubicin hydrochloride (DOX) as a pH-responsive switch [221].

Yuan et al. developed a nanoassembled drug delivery platform for antitumor therapy based on host-guest relations between cyclodextrin (CD) modified poly(acrylic acid) (PCDAA) and paclitaxel (PTX). In H22 tumor-bearing mice, PCDAA-PTX NPs can successfully target the tumor site due to their improved permeability and retention effect. PCDAA-PTX NPs have better effectiveness in suppressing tumor formation in vivo than commercially available anticancer medicines [222].

A magnetic cisplatin-encapsulated nanocapsule with a cisplatin-PAA core in an amphiphilic polyvinyl alcohol/iron oxide nanoparticles shell is made double emulsion to give excellent loading efficiency and regulated drug release. A549 tumor-bearing mice showed antitumor effectiveness with minimal adverse effects [223]. Lee et al. studied the anticancer efficacy of nanoparticles made from poly(methyl methacrylate-co-acrylic acid), including cisplatin in vitro and in vivo [224].

5.4. Cancer Theranostic

Integrating multimodal imaging and therapeutic functionalities into a nanoplatform has been identified as a viable cancer treatment method. However, several obstacles remain, such as instability and the difficult synthesis process. Zhao prepared clearable MnCo_2O_4 nanodots modified with PAA as nanoagents for T_1/T_2 bimodal MRI imaging-guided PTT. The single MnCo_2O_4 @PAA nanomaterials can be used as contrast agents for T_1/T_2 bimodal MRI, owing to their intrinsic magnetic ability and precise diagnostic information [225]. CoFe_2O_4 @PAA-FA Doxorubicin (Dox)load NPs were used to create a multifunctional theranostic nanocomposite for multifunctional cancer therapy [106].

For both controlled drug delivery and diagnostic feature, an integrated nanocomposite system was developed that contained ZIF-8 and PAA (pH-sensitive agent), manganese oxide nanoparticles (tumor diagnostic agent), and methotrexate (therapeutic agent and tumor biomarker agent) [147].

In another study, the $\text{AuNPs}@MnCO_3/Mn_3O_4$ @PAA nanoplatform is built, consisting of Au NPs doubly coated with MnCO_3/Mn_3O_4 polyacrylic acid. After that, folic acid is conjugated to the immobilized polyacrylic acid, then doxorubicin and propidium iodide are added (as fluorescence agents, targeting and therapeutic) [108].

The preparation of PAA-prussian blue-Au aggregate janus nanoparticles has been reported. This heterostructure also adds drug loading functionality, which can be used in computed tomography imaging-guided chemotherapy, and enhanced photothermal therapy promotes tumor inhibition [226].

Zhao et al. used a straightforward one-pot solvothermal approach to make a PAA-functionalized porous $\text{BiF}_3: \text{Yb, Er}$ nanocarrier. As a result, carboxyl-functionalized $\text{BiF}_3: \text{Yb, Er}$ is projected to be an excellent choice for temperature sensing and multifunctional theranostic nanoplatforms development [227]. A multifunctional core-shell contrast agent made of PAA/calcium phosphate (CaP) a shell and spherical Au nanoclusters assemblies as core have developed by Li et al. Furthermore, the doxorubicin-loaded nanoparticles may be used as synergetic pH-sensitive drug delivery vehicles in vivo for dual-modal fluorescence imaging and computed tomography-guided liver cancer treatment [228].

A repeatable and straightforward synthetic technique synthesizes PAA/mesoporous silica shell nanoparticles with gold nanoclusters aggregation and increased fluorescence characteristics. In vitro and in vivo, the as-prepared NPs were used as new theranostic agents for liver cancer chemotherapy and synergistic fluorescence/X-ray computed tomography imaging [113].

Wu et al. developed hybrid PAA- Fe_3O_4 nanogels that can be used for both drug delivery and magnetic resonance imaging. An in situ co-precipitation method encapsulated superparamagnetic Fe_3O_4 nanoparticles inside porous PAA nanogels with high drug loading release [140].

Nanobubbles have the potential to be novel theranostic systems for ultrasound, magnetic resonance imaging (MRI), combined high-intensity targeted ultrasound-triggered drug release, and magnetic targeting for the treatment of cancer. A single-step emulsion approach was used to make nanobubble-based dual contrast enhancement agents from thermosensitive F127, and PAA stabilized with superparamagnetic iron oxide nanoparticles and encapsulated with perfluorobutane. This nanobubble system's combination of functions makes it a potent and practical new tool for achieving effective cancer treatment and *in vivo* tumor imaging [229].

5.5. Tissue Engineering

An electrospun nanofiber (NFs) have shown excellent biomedical application such as controlled drug release, wound dressing, and tissue engineering. It also could be a promising candidate for postoperative chemotherapy. Hajikhani et al. reported the encapsulating properties of nanofibers derived from electrospinning of copolymers of PAA, polylactic acid, cellulose acetate, and polyethylene oxide for controlled release lycopene [230]. Khajeh et al. reported using biocompatible nanofibers derived from electrospinning of PAA, poloxamer, and polyurethane for wound dressing. The MTT experiment demonstrated that the generated NFs were non-toxic to the cells. The cell adhesion investigation revealed that the developed NFs could be used as a platform for proliferation and cell adhesion [231].

Ghaffari-Bohlouli et al. created molecularly imprinted polymer nanoparticles from an electrospun blend of PAA and poly(L-lactide-D, L-lactide) as well as poly(2-hydroxyethyl methacrylate) to form nanofibers with an average diameter of 237 nm for bone tissue engineering applications [232].

Due to its remarkable properties, such as excellent biocompatibility, minimal frictional behavior, and high water content, poly(vinyl alcohol) hydrogel has been regarded as a suitable cartilage replacement material. However, PVA hydrogel's lack of mechanical characteristics and cytocompatibility are two significant challenges to its use as a cartilage substitute. To counteract these issues, PAA has been added to the PVA hydrogel. PVA/PAA hydrogel offers comparable biocompatibility to pure PVA hydrogel and much better cell adherence. As cartilage tissue substitutes, these biocompatible composite hydrogels provide a lot of potential [233].

Various polymers and polymer-based materials, including PAA and its derivatives, have been extensively described in biomedical applications. Medical probes for analysis, biocidal actions against various diseases, hand-held water filters, surface coatings, and fibrous disinfectants are all made with these materials [234]. For example, Nurkeeva and colleagues examined the antibacterial activities of PAA and its derivatives as well as the production of PAA complexes with streptomycin sulfate [235]. Larsson and coworkers developed composite films based on biodegradable polyhydroxybutyrate (PHB) and PAA nanogels for bone-tissue engineering applications [236]. Based on the radiation-induced inter- and intramolecular cross-linking of the inter-polymer complex of PAA and polyacrylamide (PAAm), Ghorbaniazar investigated the formation of nano-sized polymeric gels. MTT assay was used to assess and prove the biocompatibility of nanogels [237].

5.6. Antimicrobial Applications

Antibiotic-resistant microorganisms have become a significant public health issue. Biofilms are the primary cause of hospital-acquired infections and illnesses [238,239]. Once developed, it is challenging to remove biofilms because they feature antimicrobial defense systems [240,241]. Antimicrobial surfaces must kill or repel germs before settling and forming a biofilm [242–244]. Gratzyl et al. used anionic polymerization with acid as a catalyst to prepare diblock copolymers based on PAA and poly(styrene) and PAA and poly(methyl methacrylate) [245]. Antibacterial activity against pathogenic microorganisms such as *S. aureus*, *E. coli*, and *P. aeruginosa* has been demonstrated. The bactericidal activity of diblock copolymers increased as the acrylic acid content increased.

Interactions between negatively charged membrane groups and negatively charged acidic components are believed to emerge via the formation of salt bridges between divalent counter ions and acids such as Mg^{2+} and Ca^{2+} , which balance the charge of the membrane on the surface of bacteria [246]. Multivalent carboxylic acids are likely to form chelates with Mg^{2+} and Ca^{2+} , destabilizing the membrane and potentially leading to cell death.

The acidic ion-exchange capacity of PAA is due to acid dissociation, which makes several deprotonated carboxylic groups available in slightly acidic circumstances and is pH-dependent [247]. Since the amount of COO^- in this range is significant and provides a high affinity for cations and a high negative charge density, the best ion-exchange ratios of PAA can be produced in the pH 4.5–6. As a result, the ion-exchange potential of the material, which is defined by the polymer's PAA content, which defines the cation affinity and negative surface charge, is the major determinant of antibacterial action. Sethy et al. synthesized PAA/GO/Ag nanocomposites in aqueous environments using an in-situ polymerization technique. It has shown excellent antibacterial activity against pathogenic bacteria [248].

According to Gratzl et al., the presence of PAA in the copolymer and slightly acidic conditions are essential for the material's antibacterial activity, but counter-ions significantly limit its efficacy. These findings lead us to believe that the bactericidal action of the copolymer is due to an ion-exchange effect [249]. The antimicrobial activities of polymeric composites based on PAA and zinc were investigated using in situ solvothermal methods against pathogenic bacteria such as *B. subtilis* and *E. coli* and fungi such as *S. cerevisiae* [250].

Shibraen et al. reported that interactions with polyacid groups resulted in doping copper, iron, and silver metal ions into polyelectrolyte multilayer matrix. Cationic guar gum /PAA nanofilms loaded with Ag^+ displayed strong antibacterial activity and could be exploited as a coating material for medical devices [251].

Previously, Nie et al. described the high-temperature synthesis of oleate-capped iron oxide nanoparticles (OIONPs), followed by a ligand exchange reaction between sodium polyacrylate and OIONPs to prepare PAA capped iron oxide nanoparticles. It was discovered to have potent antibacterial properties against *E. coli* and *S. aureus* [252]. Xu et al. developed a programmed antibacterial and remineralization technique for treating dental cavities using alendronate-grafted PAA /zinc-substituted hydroxyapatite hybrid nanoneedles [253]. Compared to PAA alone, the antibacterial capabilities of silver/gum acacia/PAA nanocomposite hydrogels have greatly improved [254]. A one-step hydrothermal deposition approach was used for coating applications to synthesize a PAA/gentamicin sulfate/hydroxyapatite. The antibacterial activity against *S. aureus* was determined using the plate-counting method [255].

Electrospinning is used to produce random and aligned PAA/PVA nanofiber scaffolds treated with cold atmospheric plasma. It has shown reasonably good antibacterial activity against *E. coli* [256]. Dil et al. reported the development of a nanocomposite hydrogel based on PAA, gelatin, and nanosilver, which demonstrated great antibacterial activity against harmful bacteria such as *S. aureus* and *E. coli* [257].

6. Compatibility and Biodegradability

In the biomedical field, biocompatibility and biodegradability are the main features of any material to be used [258]. PAA is a superabsorbent water-soluble polymer and is extensively used in several applications such as tissue engineering, disposable diapers [259], release devices [260], membranes [261], toothpaste [262], ion exchange resins [263], etc. Compatibility of PAA/Starch blends was studied and revealed that the glycerol's incorporation into the mixture was responsible for the enhancement in hydrogen bonding between starch and PAA. This stiffness was enhanced by increasing the content of starch. The PAA/Starch blends were found fully amorphous and partially miscible [264]. PAA was crosslinked with dextrin to synthesize the biocompatible crosslinked hydrogel of c-Dxt/PAA for the sustained release of ciprofloxacin and ornidazole. In the biodegradation studies, it was noticed that the mass of c-Dxt/PAA was degraded progressively, which was

done was lysozyme by glycosidic bond's enzymatic hydrolysis by the hexameric sugar ring binding sites of the lysozyme. The degradation rates were diminished between 7 to 21 days once the reduction in the suitable site occurred [265]. Cytotoxicity studies of coated liposomes with PAA nanocapsules suggested less toxicity for PAA coated than without coating, suggesting its more biocompatibility [93]. Cytotoxicity studies for PAA nanocapsules were performed with A549 cancer cells and revealed negligible cytotoxicity, demonstrating nanocapsules' biocompatibility at all concentrations. Also, the IC_{50} values were found lower, unveiled the possibility of more accumulation of PAA nanocapsules in the cells and can be used in vivo studies. The authors also studied the biocompatibility in in-vivo and suggested an electrostatic interaction between carboxylic acid of PAA and CDDP that improved the release of CDDP. The blood circulation time of these nanocapsules was increased compared to free drugs, and a 10-fold increase in the carrier for tumor accumulation revealed higher in-vivo antitumor activity. Therefore, PAA-CDDP combination with magnetic targeting was a better choice without significant bodyweight loss because of the effect of magnetic targeting [223]. The degradability of the PAA/PU semi-interpenetrating polymer networks was studied equally in normal and accelerated conditions. When the hydrophilic semi-interpenetrating polymer networks fraction was increased, the degradability was also found to be increased in three steps: incubation, induction, and erosion stage [12].

7. Conclusions, Challenges

Polymers have played a vital part in improving drug carriers by offering the controllable release of the encapsulated agent in a steady dosage over extended durations and controllable delivery of both hydrophobic and hydrophilic drugs. On the other hand, polymers that may modify their properties in response to environmental variables have recently received much interest. These polymers are stimuli-responsive materials because their functional groups make them extremely sensitive to their surroundings. PAA and its nanoconjugates could be regarded as stimuli-responsive platforms that make them ideal for drug delivery and antimicrobial applications.

The being safe of PAA-coated materials for biomedical applications should be more scientifically studied. Although PAA has admirable biocompatibility, the toxicity of these NPs for biological organisms should be approved in cell and animal experiments. Additionally, the time and mechanism required for the PAA drug delivery platform for a specific cellular compartment or tissue should be fully addressed.

8. Future Prospective

Nowadays, the primary objectives in this sector are to allow and promote more research activities aimed at developing competitive and translatable products. With this in mind, an open-minded and multidisciplinary approach may lead to the speedy and effective translation of developing PAA drug delivery systems shortly. PAA and its derived nanoparticles can be used as carrier materials for nano delivery systems and have many biomedical applications, such as drug delivery, vaccine delivery, antibacterial agent, and wound healing. Also, researchers should conduct in-depth studies on new usages for chitosan and also find out more about human-related effects through animal experiments. PAA and its derived nanoparticles will draw more and more attention and will have unlimited application prospects. Of course, merging biological and synthetic viewpoints will give a new perspective for the development of more effective polymeric nanoplateforms.

Author Contributions: Conceptualization, H.A. and M.B.; methodology, M.B.; software, M.D.S.; validation, M.B., P.Z. and N.P.S.C.; formal analysis, S.J.; investigation, M.R.A. and S.J.; resources, H.A.; data curation, M.B.; writing—original draft preparation, M.B.; writing—review and editing, M.B. and H.A. and M.R.A.; visualization, P.Z.; supervision, M.B.; project administration, H.A.; funding acquisition, M.B. All authors have read and agreed to the published version of the manuscript.

Funding: This research received no external funding.

Institutional Review Board Statement: Not applicable.

Informed Consent Statement: Not applicable.

Data Availability Statement: The data presented in this study are available on request from the corresponding author.

Conflicts of Interest: The authors declare no conflict of interest.

References

1. Suárez-García, S.; Solórzano, R.; Alibés, R.; Busqué, F.; Novio, F.; Ruiz-Molina, D. Antitumour activity of coordination polymer nanoparticles. *Coord. Chem. Rev.* **2021**, *441*, 213977. [[CrossRef](#)]
2. Daneshvari, G.; Yousefi, A.R.; Mohammadi, M.; Banibairami, S.; Shariati, P.; Rahdar, A.; Kyzas, G.Z. Controlled-release Formulations of Trifluralin Herbicide by Interfacial Polymerization as a Tool for Environmental Hazards. *Biointerface Res. Appl. Chem.* **2021**, *11*, 13866–13877.
3. Rauf, A.; Tabish, T.A.; Ibrahim, I.M.; ul Hassan, M.R.; Tahseen, S.; Sandhu, M.A.; Shahnaz, G.; Rahdar, A.; Cucchiari, M.; Pandey, S. Design of Mannose-Coated Rifampicin nanoparticles modulating the immune response and Rifampicin induced hepatotoxicity with improved oral drug delivery. *Arab. J. Chem.* **2021**, *14*, 103321. [[CrossRef](#)]
4. Rahdar, S.; Rahdar, A.; Sattari, M.; Hafshejani, L.D.; Tolkou, A.K.; Kyzas, G.Z. Barium/cobalt@ polyethylene glycol nanocomposites for dye removal from aqueous solutions. *Polymers* **2021**, *13*, 1161. [[CrossRef](#)] [[PubMed](#)]
5. Zaquen, N.; Rubens, M.; Corrigan, N.; Xu, J.; Zetterlund, P.B.; Boyer, C.; Junkers, T. Polymer synthesis in continuous flow reactors. *Prog. Polym. Sci.* **2020**, *107*, 101256. [[CrossRef](#)]
6. Kariduraganavar, M.Y.; Kittur, A.A.; Kamble, R.R. Polymer synthesis and processing. In *Natural and Synthetic Biomedical Polymers*; Elsevier: Amsterdam, The Netherlands, 2014; pp. 1–31.
7. Hacker, M.C.; Krieghoff, J.; Mikos, A.G. Synthetic polymers. In *Principles of Regenerative Medicine*; Elsevier: Amsterdam, The Netherlands, 2019; pp. 559–590.
8. Pavlinec, J.; Novák, I.; Rychlý, J.; Kleinová, A.; Nógellová, Z.; Preťo, J.; Vanko, V.; Žigo, O.; Chodák, I. Hot melt adhesives prepared by grafting of acrylic and crotonic acids onto metallocene ethylene-octene copolymers. *J. Plast. Film. Sheeting* **2019**, *35*, 239–259. [[CrossRef](#)]
9. Dashtizadeh, A.; Abdouss, M.; Khorassani, M.; Mahdavi, H. Preparation of silica-filled water-based acrylic nanocomposite paints with improved scratch resistance. *J. Plast. Film. Sheeting* **2012**, *28*, 120–135. [[CrossRef](#)]
10. Savaskan Yilmaz, S.; Yildirim, N.; Misir, M.; Misirlioglu, Y.; Celik, E. Synthesis, Characterization of a New Polyacrylic Acid Superabsorbent, Some Heavy Metal Ion Sorption, the Adsorption Isotherms, and Quantum Chemical Investigation. *Materials* **2020**, *13*, 4390. [[CrossRef](#)]
11. Yee, S.Y.Y. Medicinal properties of bioactive compounds and antioxidant activity in *Durio zibethinus*. *Malays. J. Sustain. Agric. (MJSA)* **2021**, *5*, 82–89. [[CrossRef](#)]
12. Zenozi, S.; Sadeghi, G.M.M.; Rafiee, M. Synthesis and characterization of biocompatible semi-interpenetrating polymer networks based on polyurethane and cross-linked poly (acrylic acid). *Eur. Polym. J.* **2020**, *140*, 109974. [[CrossRef](#)]
13. Zuo, Y.; Yang, W.; Zhang, K.; Chen, Y.; Yin, X.; Liu, Y. Experimental and theoretical studies of carboxylic polymers with low molecular weight as inhibitors for calcium carbonate scale. *Crystals* **2020**, *10*, 406. [[CrossRef](#)]
14. Mori, H.; Müller, A.H.; Klee, J.E. Intelligent colloidal hybrids via reversible pH-induced complexation of polyelectrolyte and silica nanoparticles. *J. Am. Chem. Soc.* **2003**, *125*, 3712–3713. [[CrossRef](#)] [[PubMed](#)]
15. Shimizu, T.; Masuda, M.; Minamikawa, H. Supramolecular nanotube architectures based on amphiphilic molecules. *Chem. Rev.* **2005**, *105*, 1401–1444. [[CrossRef](#)] [[PubMed](#)]
16. Ma, Y.; Dong, J.; Bhattacharjee, S.; Wijeratne, S.; Bruening, M.L.; Baker, G.L. Increased protein sorption in poly (acrylic acid)-containing films through incorporation of comb-like polymers and film adsorption at low pH and high ionic strength. *Langmuir* **2013**, *29*, 2946–2954. [[CrossRef](#)]
17. Spagnol, C.; Rodrigues, F.H.; Pereira, A.G.; Fajardo, A.R.; Rubira, A.F.; Muniz, E.C. Superabsorbent hydrogel composite made of cellulose nanofibrils and chitosan-graft-poly (acrylic acid). *Carbohydr. Polym.* **2012**, *87*, 2038–2045. [[CrossRef](#)]
18. Takada, K.; Iida, T.; Kawanishi, Y.; Yasui, T.; Yuchi, A. An electrochemical actuator based on reversible changes in volume of poly (acrylic acid) gel induced by quinone redox. *Sens. Actuators B Chem.* **2011**, *160*, 1586–1592. [[CrossRef](#)]
19. Hisamatsu, N.; Iida, T.; Yasui, T.; Takada, K.; Yuchi, A. Double-side coated electrochemical actuator based on changes in volume of poly (acrylic acid) gel. *Sens. Actuators B Chem.* **2014**, *203*, 289–295. [[CrossRef](#)]
20. Changez, M.; Koul, V.; Krishna, B.; Dinda, A.K.; Choudhary, V. Studies on biodegradation and release of gentamicin sulphate from interpenetrating network hydrogels based on poly (acrylic acid) and gelatin: In vitro and in vivo. *Biomaterials* **2004**, *25*, 139–146. [[CrossRef](#)]
21. Khanlari, S.; Dubé, M.A. Bioadhesives: A review. *Macromol. React. Eng.* **2013**, *7*, 573–587. [[CrossRef](#)]
22. Dai, Y.; Zhang, C.; Cheng, Z.; Li, C.; Kang, X.; Yang, D.; Lin, J. pH-responsive drug delivery system based on luminescent CaF₂:Ce³⁺/Tb³⁺-poly (acrylic acid) hybrid microspheres. *Biomaterials* **2012**, *33*, 2583–2592. [[CrossRef](#)]

23. Babiker, D.M.; Zhu, L.; Yagoub, H.; Xu, X.; Zhang, X.; Shibraen, M.H.; Yang, S. Hydrogen-bonded methylcellulose/poly (acrylic acid) complex membrane for oil-water separation. *Surf. Coat. Technol.* **2019**, *367*, 49–57. [[CrossRef](#)]
24. Abd Alsaheb, R.A.; Aladdin, A.; Othman, N.Z.; Abd Malek, R.; Leng, O.M.; Aziz, R.; El Enshasy, H.A. Recent applications of polylactic acid in pharmaceutical and medical industries. *J. Chem. Pharm. Res* **2015**, *7*, 51–63.
25. Jiang, L.; Gao, L.; Wang, X.; Tang, L.; Ma, J. The application of mucoadhesive polymers in nasal drug delivery. *Drug Dev. Ind. Pharm.* **2010**, *36*, 323–336. [[CrossRef](#)] [[PubMed](#)]
26. Swilem, A.E.; Elshazly, A.H.; Hamed, A.A.; Hegazy, E.-S.A.; Abd El-Rehim, H.A. Nanoscale poly (acrylic acid)-based hydrogels prepared via a green single-step approach for application as low-viscosity biomimetic fluid tears. *Mater. Sci. Eng. C* **2020**, *110*, 110726. [[CrossRef](#)] [[PubMed](#)]
27. Partenhauser, A.; Bernkop-Schnürch, A. Mucoadhesive polymers in the treatment of dry X syndrome. *Drug Discov. Today* **2016**, *21*, 1051–1062. [[CrossRef](#)] [[PubMed](#)]
28. Monirifard, R.; Abolhasani, M.; Tahani, B.; Fathi, A.; Choobdaran, A. Relationship of Personality Traits and Patient Satisfaction with Fixed Implant Prosthodontic Treatments. *J. Iran. Dent. Assoc.* **2019**, *31*, 182–188. [[CrossRef](#)]
29. Mosharraf, R.; Molaie, P.; Fathi, A.; Isler, S. Investigating the Effect of Nonrigid Connectors on the Success of Tooth-and-Implant-Supported Fixed Partial Prostheses in Maxillary Anterior Region: A Finite Element Analysis (FEA). *Int. J. Dent.* **2021**, *2021*, 5977994. [[CrossRef](#)]
30. Maalekipour, M.; Safari, M.; Barekain, M.; Fathi, A. Effect of Adhesive Resin as a Modeling Liquid on Elution of Resin Composite Restorations. *Int. J. Dent.* **2021**, *2021*, 3178536. [[CrossRef](#)]
31. Abolhasani, M.; Givchian, P.; Fathi, A.; Goudarzi, S. Relationship of Life Satisfaction and Satisfaction with Fixed Implant-Supported Prostheses in the Elderly. *J. Iran. Dent. Assoc.* **2021**, *33*, 17–21.
32. Roostae, M.; Sheikhshoaie, I. Low-temperature synthesis of hetero-structures of magnetically separable iron oxide@ Au-rGO nanocomposite for efficient degradation of organic dye under visible light irradiation. *Environ. Res.* **2022**, *205*, 112510. [[CrossRef](#)]
33. Roostae, M.; Sheikhshoaie, I. Fabrication of a sensitive sensor for determination of xanthine in the presence of uric acid and ascorbic acid by modifying a carbon paste sensor with Fe₃O₄@ Au core-shell and an ionic liquid. *J. Food Meas. Charact.* **2022**, *16*, 731–739. [[CrossRef](#)]
34. Hooshmand, S.; Hayat, S.M.G.; Ghorbani, A.; Khatami, M.; Pakravanan, K.; Darroudi, M. Preparation and Applications of Superparamagnetic Iron Oxide Nanoparticles in Novel Drug Delivery Systems: An Overview Article. *Curr. Med. Chem.* **2022**, *28*, 777–799. [[CrossRef](#)]
35. Roostae, M.; Sheikhshoaie, I. A novel, sensitive and selective nanosensor based on graphene nanoribbon-cobalt ferrite nanocomposite and 1-methyl-3-butylimidazolium bromide for detection of vanillin in real food samples. *J. Food Meas. Charact.* **2022**, *16*, 523–532. [[CrossRef](#)]
36. Roostae, M.; Sheikhshoaie, I.; Karimi-Maleh, H. Fe₃O₄@ Au-rGO Nanocomposite/Ionic Liquid Modified Sensor for Ultrasensitive and Selective Sensing of Doxorubicin. *Top. Catal.* **2022**, 1–10. [[CrossRef](#)]
37. Ebadian, B.; Fathi, A.; Savoj, M. In Vitro Evaluation of the Effect of Different Luting Cements and Tooth Preparation Angle on the Microleakage of Zirconia Crowns. *Int. J. Dent.* **2021**, *2021*, 8461579. [[CrossRef](#)] [[PubMed](#)]
38. Kargozar, S.; Mozafari, M. Nanotechnology and Nanomedicine: Start small, think big. *Mater. Today Proc.* **2018**, *5*, 15492–15500. [[CrossRef](#)]
39. Roostae, M.; Sheikhshoaie, I. Magnetic nanoparticles; synthesis, properties and electrochemical application: A review. *Curr. Biochem. Eng.* **2020**, *6*, 91–102. [[CrossRef](#)]
40. Xu, M.; Zhu, J.; Wang, F.; Xiong, Y.; Wu, Y.; Wang, Q.; Weng, J.; Zhang, Z.; Chen, W.; Liu, S. Improved in vitro and in vivo biocompatibility of graphene oxide through surface modification: Poly (acrylic acid)-functionalization is superior to PEGylation. *ACS Nano* **2016**, *10*, 3267–3281. [[CrossRef](#)]
41. Jing, Z.; Xu, A.; Liang, Y.-Q.; Zhang, Z.; Yu, C.; Hong, P.; Li, Y. Biodegradable poly (acrylic acid-co-acrylamide)/poly (vinyl alcohol) double network hydrogels with tunable mechanics and high self-healing performance. *Polymers* **2019**, *11*, 952. [[CrossRef](#)]
42. Mutar, M.A.; Kmal, R.K. Preparation of copolymer of acrylamide and acrylic acid and its application for slow release sodium nitrate fertilizer. *Al-Qadisiyah J. Pure Sci.* **2012**, *17*, 71–83.
43. Gao, J.; Penlidis, A. A comprehensive simulator/database package for reviewing free-radical copolymerizations. *J. Macromol. Sci. Part C* **1998**, *38*, 651–780. [[CrossRef](#)]
44. Sennakesavan, G.; Mostakhdemin, M.; Dkhar, L.; Seyfoddin, A.; Fatihhi, S. Acrylic acid/acrylamide based hydrogels and its properties-A review. *Polym. Degrad. Stab.* **2020**, *180*, 109308. [[CrossRef](#)]
45. Ishizone, T.; Sugiyama, K.; Hirao, A. *Anionic Polymerization of Protected Functional Monomers*; Elsevier: Amsterdam, The Netherlands, 2012.
46. Satoh, K.; Kamigaito, M.; Sawamoto, M. *Transition Metal Complexes for Metal-Catalyzed Atom Transfer Controlled/Living Radical Polymerization*; Elsevier: Amsterdam, The Netherlands, 2012.
47. Matyjaszewski, K.; Spaswick, J. *Copper-Mediated Atom Transfer Radical Polymerization*; Elsevier: Amsterdam, The Netherlands, 2012.
48. Kausar, A. Poly (acrylic acid) nanocomposites: Design of advanced materials. *J. Plast. Film Sheeting* **2020**, *36*, 409–428. [[CrossRef](#)]
49. Masuda, T.; Takai, M. Structure and properties of thermoresponsive gels formed by RAFT polymerization: Effect of the RAFT agent content. *Polym. J.* **2020**, *52*, 1407–1412. [[CrossRef](#)]

50. Chanprapanon, W.; Chitpong, N. Functionalized nonwoven Nylon fabrics for cadmium ion exchange applications. *Eng. Appl. Sci. Res.* **2020**, *47*, 222–231.
51. Chrisostomo, D.A.; Strazzi-Sahyon, H.B.; Briso, A.L.F.; Dos Santos, P.H. Efficacy of Polyacrylic Acid as a Conditioning Agent on the Bond Strength of Self-adhesive Resin Cements to Dental Enamel. *Oral Health Prev. Dent.* **2020**, *18*, 747–756.
52. Jing, X.; Feng, P.; Chen, Z.; Xie, Z.; Li, H.; Peng, X.-F.; Mi, H.-Y.; Liu, Y. Highly Stretchable, Self-Healable, Freezing-Tolerant, and Transparent Polyacrylic Acid/Nanochitin Composite Hydrogel for Self-Powered Multifunctional Sensors. *ACS Sustain. Chem. Eng.* **2021**, *9*, 9209–9220. [[CrossRef](#)]
53. Schilli, C.M.; Zhang, M.; Rizzardo, E.; Thang, S.H.; Chong, Y.; Edwards, K.; Karlsson, G.; Müller, A.H. A new double-responsive block copolymer synthesized via RAFT polymerization: Poly (N-isopropylacrylamide)-b lock-poly (acrylic acid). *Macromolecules* **2004**, *37*, 7861–7866. [[CrossRef](#)]
54. Yigit, F.; Güven, O. A kinetic investigation of radiation induced bulk polymerization of acrylic acid. *Int. J. Radiat. Appl. Instrum. Part C Radiat. Phys. Chem.* **1989**, *33*, 97–101. [[CrossRef](#)]
55. Kahveci, M.; Yagci, Y.; Avgeropoulos, A.; Tsitsilianis, C. *Well-Defined Block Copolymers*; Elsevier: Amsterdam, The Netherlands, 2012.
56. Patten, T.E.; Matyjaszewski, K. Atom transfer radical polymerization and the synthesis of polymeric materials. *Adv. Mater.* **1998**, *10*, 901–915. [[CrossRef](#)]
57. Couvreur, L.; Lefay, C.; Bellene, J.; Charleux, B.; Guerret, O.; Magnet, S. First Nitroxide-Mediated Controlled Free-Radical Polymerization of Acrylic Acid. *Macromolecules* **2003**, *36*, 8260. [[CrossRef](#)]
58. Ladavière, C.; Dörr, N.; Claverie, J.P. Controlled radical polymerization of acrylic acid in protic media. *Macromolecules* **2001**, *34*, 5370–5372. [[CrossRef](#)]
59. Sütekin, S.D.; Güven, O. Preparation of poly (tert-butyl acrylate)-poly (acrylic acid) amphiphilic copolymers via radiation-induced reversible addition–fragmentation chain transfer mediated polymerization of tert-butyl acrylate. *Polym. Int.* **2020**, *69*, 693–701. [[CrossRef](#)]
60. Yan, L.; Ji, J.; Xie, D.; Li, W.; Zhang, G. Surfactant-free synthesis of amphiphilic copolymer of poly (styrene-co-acrylamide) in aqueous emulsion with the assistance of ultrasound. *Polym. Adv. Technol.* **2008**, *19*, 221–228. [[CrossRef](#)]
61. Loiseau, J.; Doërr, N.; Suau, J.; Egraz, J.; Llauro, M.; Ladavière, C.; Claverie, J. Synthesis and characterization of poly (acrylic acid) produced by RAFT polymerization. Application as a very efficient dispersant of CaCO₃, kaolin, and TiO₂. *Macromolecules* **2003**, *36*, 3066–3077. [[CrossRef](#)]
62. Millard, P.E.; Barner, L.; Stenzel, M.H.; Davis, T.P.; Barner-Kowollik, C.; Müller, A.H. RAFT Polymerization of N-Isopropylacrylamide and Acrylic Acid under γ -Irradiation in Aqueous Media. *Macromol. Rapid Commun.* **2006**, *27*, 821–828. [[CrossRef](#)]
63. Moad, G.; Chong, Y.; Postma, A.; Rizzardo, E.; Thang, S.H. Advances in RAFT polymerization: The synthesis of polymers with defined end-groups. *Polymer* **2005**, *46*, 8458–8468. [[CrossRef](#)]
64. Hassan, S.; Yasin, T. Synthesis of radiation crosslinked poly (acrylic acid) in the presence of phenyltriethoxysilane. *Radiat. Phys. Chem.* **2014**, *97*, 292–297. [[CrossRef](#)]
65. Barner-Kowollik, C.; Buback, M.; Charleux, B.; Coote, M.L.; Drache, M.; Fukuda, T.; Goto, A.; Klumperman, B.; Lowe, A.B.; Mcleary, J.B. Mechanism and kinetics of dithiobenzoate-mediated RAFT polymerization. I. The current situation. *J. Polym. Sci. Part A Polym. Chem.* **2006**, *44*, 5809–5831. [[CrossRef](#)]
66. Ji, J.; Jia, L.; Yan, L.; Bangal, P.R. Efficient synthesis of poly (acrylic acid) in aqueous solution via a RAFT process. *J. Macromol. Sci. Part A Pure Appl. Chem.* **2010**, *47*, 445–451. [[CrossRef](#)]
67. Liu, L.; Xu, Z.; Liu, Y.; Yin, Z.-Z.; Sheng, Y.; Ding, C.; Kong, Y. Facile synthesis of calcium carbonate/polyacrylic acid hydrogels for pH-responsive delivery of cytarabine. *J. Saudi Chem. Soc.* **2021**, *25*, 101344. [[CrossRef](#)]
68. Xiong, J.; Dupré, N.; Mazouzi, D.; Guyomard, D.; Roué, L.; Lestriez, B. Influence of the polyacrylic acid binder neutralization degree on the initial electrochemical behavior of a silicon/graphite electrode. *ACS Appl. Mater. Interfaces* **2021**, *13*, 28304–28323. [[CrossRef](#)] [[PubMed](#)]
69. Shukla, N.B.; Darabonia, N.; Madras, G. Ultrasonic degradation of poly (acrylic acid). *J. Appl. Polym. Sci.* **2009**, *112*, 991–997. [[CrossRef](#)]
70. Kadlubowski, S.; Grobelny, J.; Olejniczak, W.; Cichomski, M.; Ulanski, P. Pulses of fast electrons as a tool to synthesize poly (acrylic acid) nanogels. Intramolecular cross-linking of linear polymer chains in additive-free aqueous solution. *Macromolecules* **2003**, *36*, 2484–2492. [[CrossRef](#)]
71. Kumar, A.; Maity, D.; Vyas, G.; Bhatt, M.; Bhatt, S.; Paul, P. Polyacrylic acid@ zeolitic imidazolate framework-8 nanoparticles for detection and absorptive removal of cyanide from aqueous media with high efficiency. *Colloids Surf. A Physicochem. Eng. Asp.* **2021**, *617*, 126358. [[CrossRef](#)]
72. Laraib, U.; Sargazi, S.; Rahdar, A.; Khatami, M.; Pandey, S. Nanotechnology-based approaches for effective detection of tumor markers: A comprehensive state-of-the-art review. *Int. J. Biol. Macromol.* **2021**, *195*, 356–383. [[CrossRef](#)]
73. De la Garza, D.; De Santiago, F.; Materon, L.; Chipara, M.; Alcoutlabi, M. Fabrication and characterization of centrifugally spun poly (acrylic acid) nanofibers. *J. Appl. Polym. Sci.* **2019**, *136*, 47480. [[CrossRef](#)]
74. Jin, X.; Hsieh, Y.-L. pH-responsive swelling behavior of poly (vinyl alcohol)/poly (acrylic acid) bi-component fibrous hydrogel membranes. *Polymer* **2005**, *46*, 5149–5160. [[CrossRef](#)]

75. Santiago-Morales, J.; Amariei, G.; Letón, P.; Rosal, R. Antimicrobial activity of poly (vinyl alcohol)-poly (acrylic acid) electrospun nanofibers. *Colloids Surf. B Biointerfaces* **2016**, *146*, 144–151. [[CrossRef](#)]
76. Duan, Z.; Yin, Q.; Li, C.; Dong, L.; Bai, X.; Zhang, Y.; Yang, M.; Jia, D.; Li, R.; Liu, Z. Milling force and surface morphology of 45 steel under different Al₂O₃ nanofluid concentrations. *Int. J. Adv. Manuf. Technol.* **2020**, *107*, 1277–1296. [[CrossRef](#)]
77. Greindl, M.; Bernkop-Schnürch, A. Development of a novel method for the preparation of thiolated polyacrylic acid nanoparticles. *Pharm. Res.* **2006**, *23*, 2183–2189. [[CrossRef](#)] [[PubMed](#)]
78. Molnar, R.M.; Bodnar, M.; Hartmann, J.F.; Borbely, J. Preparation and characterization of poly (acrylic acid)-based nanoparticles. *Colloid Polym. Sci.* **2009**, *287*, 739–744. [[CrossRef](#)]
79. Lu, Y.; Mei, Y.; Schrinner, M.; Ballauff, M.; Möller, M.W.; Breu, J. In situ formation of Ag nanoparticles in spherical polyacrylic acid brushes by UV irradiation. *J. Phys. Chem. C* **2007**, *111*, 7676–7681. [[CrossRef](#)]
80. Müller, C.; Leithner, K.; Hauptstein, S.; Hintzen, F.; Salvenmoser, W.; Bernkop-Schnürch, A. Preparation and characterization of mucus-penetrating papain/poly (acrylic acid) nanoparticles for oral drug delivery applications. *J. Nanopart. Res.* **2013**, *15*, 1353. [[CrossRef](#)]
81. Deng, Z.J.; Liang, M.; Toth, I.; Monteiro, M.J.; Minchin, R.F. Molecular interaction of poly (acrylic acid) gold nanoparticles with human fibrinogen. *ACS Nano* **2012**, *6*, 8962–8969. [[CrossRef](#)]
82. Sanchez, L.M.; Martin, D.A.; Alvarez, V.A.; Gonzalez, J.S. Polyacrylic acid-coated iron oxide magnetic nanoparticles: The polymer molecular weight influence. *Colloids Surf. A Physicochem. Eng. Asp.* **2018**, *543*, 28–37. [[CrossRef](#)]
83. Hu, Y.; Jiang, X.; Ding, Y.; Ge, H.; Yuan, Y.; Yang, C. Synthesis and characterization of chitosan–poly (acrylic acid) nanoparticles. *Biomaterials* **2002**, *23*, 3193–3201. [[CrossRef](#)]
84. Ma, Y.-H.; Wu, S.-Y.; Wu, T.; Chang, Y.-J.; Hua, M.-Y.; Chen, J.-P. Magnetically targeted thrombolysis with recombinant tissue plasminogen activator bound to polyacrylic acid-coated nanoparticles. *Biomaterials* **2009**, *30*, 3343–3351. [[CrossRef](#)]
85. Mahdavian, A.R.; Mirrahimi, M.A.-S. Efficient separation of heavy metal cations by anchoring polyacrylic acid on superparamagnetic magnetite nanoparticles through surface modification. *Chem. Eng. J.* **2010**, *159*, 264–271. [[CrossRef](#)]
86. Couto, D.; Freitas, M.; Vilas-Boas, V.; Dias, I.; Porto, G.; Lopez-Quintela, M.A.; Rivas, J.; Freitas, P.; Carvalho, F.; Fernandes, E. Interaction of polyacrylic acid coated and non-coated iron oxide nanoparticles with human neutrophils. *Toxicol. Lett.* **2014**, *225*, 57–65. [[CrossRef](#)]
87. Cerqueira, M.A.; Pinheiro, A.C.; Silva, H.D.; Ramos, P.E.; Azevedo, M.A.; Flores-López, M.L.; Rivera, M.C.; Bourbon, A.I.; Ramos, Ó.L.; Vicente, A.A. Design of bio-nanosystems for oral delivery of functional compounds. *Food Eng. Rev.* **2014**, *6*, 1–19. [[CrossRef](#)]
88. Zhang, Y.; Hsu, B.Y.W.; Ren, C.; Li, X.; Wang, J. Silica-based nanocapsules: Synthesis, structure control and biomedical applications. *Chem. Soc. Rev.* **2015**, *44*, 315–335. [[CrossRef](#)] [[PubMed](#)]
89. Belbekhouche, S.; Mansour, O.; Carbonnier, B. Promising sub-100 nm tailor made hollow chitosan/poly (acrylic acid) nanocapsules for antibiotic therapy. *J. Colloid Interface Sci.* **2018**, *522*, 183–190. [[CrossRef](#)] [[PubMed](#)]
90. Nan, J.; Chen, Y.; Li, R.; Wang, J.; Liu, M.; Wang, C.; Chu, F. Polymeric hydrogel nanocapsules: A thermo and pH Dual-responsive carrier for sustained drug release. *Nano-Micro Lett.* **2014**, *6*, 200–208. [[CrossRef](#)]
91. Wang, R.M.; Li, G.; Zhang, H.F.; He, Y.F.; He, N.P.; Lei, Z. Preparation of albumin—PAA nanocapsules and their controlled release behavior for drugs. *Polym. Adv. Technol.* **2010**, *21*, 685–690. [[CrossRef](#)]
92. Aqil, A.; Detrembleur, C.; Gilbert, B.; Jérôme, R.; Jérôme, C. Controlled RAFT synthesis of polyacrylonitrile-b-poly (acrylic acid) diblocks as precursors of carbon nanocapsules with assistance of gold nanoparticles. *Chem. Mater.* **2007**, *19*, 2150–2154. [[CrossRef](#)]
93. Scarioti, G.D.; Lubambo, A.; Feitosa, J.P.; Sierakowski, M.R.; Bresolin, T.M.; de Freitas, R.A. Nanocapsule of cationic liposomes obtained using “in situ” acrylic acid polymerization: Stability, surface charge and biocompatibility. *Colloids Surf. B Biointerfaces* **2011**, *87*, 267–272. [[CrossRef](#)]
94. Zhang, W.-J.; Yan, Y.-Z.; Nagappan, S.; He, S.; Ha, C.-S.; Jin, Y.-S. Dual (thermo-/pH-) responsive P (NIPAM-co-AA-co-HEMA) nanocapsules for controlled release of 5-fluorouracil. *J. Macromol. Sci. Part A* **2021**, *58*, 860–871. [[CrossRef](#)]
95. Perkin, K.K.; Turner, J.L.; Wooley, K.L.; Mann, S. Fabrication of hybrid nanocapsules by calcium phosphate mineralization of shell cross-linked polymer micelles and nanocages. *Nano Lett.* **2005**, *5*, 1457–1461. [[CrossRef](#)]
96. Kurkuri, M.D.; Aminabhavi, T.M. Poly (vinyl alcohol) and poly (acrylic acid) sequential interpenetrating network pH-sensitive microspheres for the delivery of diclofenac sodium to the intestine. *J. Control. Release* **2004**, *96*, 9–20. [[CrossRef](#)]
97. Liu, M.; Zeng, G.; Wang, K.; Wan, Q.; Tao, L.; Zhang, X.; Wei, Y. Recent developments in polydopamine: An emerging soft matter for surface modification and biomedical applications. *Nanoscale* **2016**, *8*, 16819–16840. [[CrossRef](#)] [[PubMed](#)]
98. He, W.-D.; Sun, X.-L.; Wan, W.-M.; Pan, C.-Y. Multiple morphologies of PAA-b-PSt assemblies throughout RAFT dispersion polymerization of styrene with PAA macro-CTA. *Macromolecules* **2011**, *44*, 3358–3365. [[CrossRef](#)]
99. Cheng, W.; Zeng, X.; Chen, H.; Li, Z.; Zeng, W.; Mei, L.; Zhao, Y. Versatile polydopamine platforms: Synthesis and promising applications for surface modification and advanced nanomedicine. *ACS Nano* **2019**, *13*, 8537–8565. [[CrossRef](#)] [[PubMed](#)]
100. Mrówczyński, R.; Jurga-Stopa, J.; Markiewicz, R.; Coy, E.L.; Jurga, S.; Woźniak, A. Assessment of polydopamine coated magnetic nanoparticles in doxorubicin delivery. *RSC Adv.* **2016**, *6*, 5936–5943. [[CrossRef](#)]
101. Couto, D.; Freitas, M.; Porto, G.; Lopez-Quintela, M.A.; Rivas, J.; Freitas, P.; Carvalho, F.; Fernandes, E. Polyacrylic acid-coated and non-coated iron oxide nanoparticles induce cytokine activation in human blood cells through TAK1, p38 MAPK and JNK pro-inflammatory pathways. *Arch. Toxicol.* **2015**, *89*, 1759–1769. [[CrossRef](#)] [[PubMed](#)]

102. Sun, S.-L.; Lo, Y.-L.; Chen, H.-Y.; Wang, L.-F. Hybrid polyethylenimine and polyacrylic acid-bound iron oxide as a magnetoplex for gene delivery. *Langmuir* **2012**, *28*, 3542–3552. [[CrossRef](#)]
103. González-Gómez, M.A.; Belderbos, S.; Yañez-Vilar, S.; Piñeiro, Y.; Cleeren, F.; Bormans, G.; Deroose, C.M.; Gsell, W.; Himmelreich, U.; Rivas, J. Development of superparamagnetic nanoparticles coated with polyacrylic acid and aluminum hydroxide as an efficient contrast agent for multimodal imaging. *Nanomaterials* **2019**, *9*, 1626. [[CrossRef](#)]
104. Zhang, Z.; Zhuang, L.; Lin, Y.; Yan, M.; Lv, J.; Li, X.; Lin, H.; Zhu, P.; Lin, Q.; Xu, Y. Novel drug delivery system based on hollow mesoporous magnetic nanoparticles for head and neck cancers—targeted therapy in vitro and in vivo. *Am. J. Cancer Res.* **2020**, *10*, 350.
105. Rodrigues, D.; Freitas, M.; Marisa Costa, V.; Arturo Lopez-Quintela, M.; Rivas, J.; Freitas, P.; Carvalho, F.; Fernandes, E.; Silva, P. Quantitative histochemistry for macrophage biodistribution on mice liver and spleen after the administration of a pharmacological-relevant dose of polyacrylic acid-coated iron oxide nanoparticles. *Nanotoxicology* **2017**, *11*, 256–266. [[CrossRef](#)]
106. Arkaban, H.; Ebrahimi, A.K.; Yarahmadi, A.; Zarrintaj, P.; Barani, M. Development of a multifunctional system based on CoFe₂O₄@ polyacrylic acid NPs conjugated to folic acid and loaded with doxorubicin for cancer theranostics. *Nanotechnology* **2021**, *32*, 305101. [[CrossRef](#)]
107. Foroushani, M.S.; Niroumand, N.; Shervedani, R.K.; Yaghoobi, F.; Kefayat, A.; Torabi, M. A theranostic system based on nanocomposites of manganese oxide nanoparticles and a pH sensitive polymer: Preparation, and physicochemical characterization. *Bioelectrochemistry* **2019**, *130*, 107347. [[CrossRef](#)] [[PubMed](#)]
108. Arkaban, H.; Shervedani, R.K.; Yaghoobi, F.; Kefayat, A. A nanocomposite theranostic system, consisting of AuNPs@ MnCO₃/Mn₃O₄ coated with PAA and integrated with folic acid, doxorubicin, and propidium iodide: Synthesis, characterization and examination for capturing of cancer cells. *Inorg. Chem. Commun.* **2021**, *128*, 108566. [[CrossRef](#)]
109. Cho, M.H.; Choi, E.-S.; Kim, S.; Goh, S.-H.; Choi, Y. Redox-responsive manganese dioxide nanoparticles for enhanced MR imaging and radiotherapy of lung cancer. *Front. Chem.* **2017**, *5*, 109. [[CrossRef](#)] [[PubMed](#)]
110. Aslam Khan, M.U.; Mehboob, H.; Abd Razak, S.I.; Yahya, M.Y.; Mohd Yusof, A.H.; Ramlee, M.H.; Sahaya Anand, T.J.; Hassan, R.; Aziz, A.; Amin, R. Development of polymeric nanocomposite (xyloglucan-co-methacrylic acid/hydroxyapatite/sio₂) scaffold for bone tissue engineering applications—In-vitro antibacterial, cytotoxicity and cell culture evaluation. *Polymers* **2020**, *12*, 1238. [[CrossRef](#)]
111. Pan, S.; Xing, H.; Fu, X.; Yu, H.; Yang, Z.; Yang, Y.; Sun, W. The effect of photothermal therapy on osteosarcoma with polyacrylic acid-coated gold nanorods. *Dose-Response* **2018**, *16*, 1559325818789841. [[CrossRef](#)]
112. Li, G.; Chen, Y.; Zhang, L.; Zhang, M.; Li, S.; Li, L.; Wang, T.; Wang, C. Facile approach to synthesize gold nanorod@ polyacrylic acid/calcium phosphate yolk-shell nanoparticles for dual-mode imaging and pH/NIR-responsive drug delivery. *Nano-Micro Lett.* **2018**, *10*, 7. [[CrossRef](#)]
113. Wu, X.; Li, L.; Zhang, L.; Wang, T.; Wang, C.; Su, Z. Multifunctional spherical gold nanocluster aggregate@ polyacrylic acid@ mesoporous silica nanoparticles for combined cancer dual-modal imaging and chemo-therapy. *J. Mater. Chem. B* **2015**, *3*, 2421–2425. [[CrossRef](#)]
114. Tian, C.; Zhu, L.; Lin, F.; Boyes, S.G. Poly (acrylic acid) bridged gadolinium metal-organic framework-gold nanoparticle composites as contrast agents for computed tomography and magnetic resonance bimodal imaging. *ACS Appl. Mater. Interfaces* **2015**, *7*, 17765–17775. [[CrossRef](#)]
115. Mazloomi-Rezvani, M.; Salami-Kalajahi, M.; Roghani-Mamaqani, H. Fabricating core (Au)-shell (different stimuli-responsive polymers) nanoparticles via inverse emulsion polymerization: Comparing DOX release behavior in dark room and under NIR lighting. *Colloids Surf. B Biointerfaces* **2018**, *166*, 144–151. [[CrossRef](#)]
116. Song, C.; Dou, Y.; Yuwen, L.; Sun, Y.; Dong, C.; Li, F.; Yang, Y.; Wang, L. A gold nanoflower-based traceable drug delivery system for intracellular SERS imaging-guided targeted chemo-phototherapy. *J. Mater. Chem. B* **2018**, *6*, 3030–3039. [[CrossRef](#)]
117. Li, L.; Liu, C.; Zhang, L.; Wang, T.; Yu, H.; Wang, C.; Su, Z. Multifunctional magnetic-fluorescent eccentric-(concentric-Fe₃O₄@ SiO₂)@ polyacrylic acid core-shell nanocomposites for cell imaging and pH-responsive drug delivery. *Nanoscale* **2013**, *5*, 2249–2253. [[CrossRef](#)] [[PubMed](#)]
118. Xia, Z.; Fu, Y.; Gu, T.; Li, Y.; Liu, H.; Ren, Z.; Li, X.; Han, G. Fibrous CaF₂: Yb, Er@ SiO₂-PAA ‘tumor patch’ with NIR-triggered and trackable DOX release. *Mater. Des.* **2017**, *119*, 85–92. [[CrossRef](#)]
119. Alahri, M.B.; Arshadizadeh, R.; Raeisi, M.; Khatami, M.; Sajadi, M.S.; Abdelbasset, W.K.; Akhmadeev, R.; Iravani, S. Theranostic applications of metal-organic frameworks (MOFs)-based materials in brain disorders: Recent advances and challenges. *Inorg. Chem. Commun.* **2021**, *134*, 108997. [[CrossRef](#)]
120. Bazzazzadeh, A.; Dizaji, B.F.; Kianinejad, N.; Nouri, A.; Irani, M. Fabrication of poly (acrylic acid) grafted-chitosan/polyurethane/magnetic MIL-53 metal organic framework composite core-shell nanofibers for co-delivery of temozolomide and paclitaxel against glioblastoma cancer cells. *Int. J. Pharm.* **2020**, *587*, 119674. [[CrossRef](#)] [[PubMed](#)]
121. Tran, V.A.; Lee, S.-W. pH-triggered degradation and release of doxorubicin from zeolitic imidazolate framework-8 (ZIF8) decorated with polyacrylic acid. *RSC Adv.* **2021**, *11*, 9222–9234. [[CrossRef](#)]
122. Bardajee, G.R.; Sharifi, M.; Torkamani, H.; Vancaeyzeele, C. Synthesis of magnetic multi walled carbon nanotubes hydrogel nanocomposite based on poly (acrylic acid) grafted onto salep and its application in the drug delivery of tetracycline hydrochloride. *Colloids Surf. A Physicochem. Eng. Asp.* **2021**, *616*, 126350. [[CrossRef](#)]

123. Chen, Y.; Qi, Y.; Liu, B. Polyacrylic acid functionalized nanographene as a nanocarrier for loading and controlled release of doxorubicin hydrochloride. *J. Nanomater.* **2013**, *2013*, 345738. [[CrossRef](#)]
124. Sgarlata, C.; D'Urso, L.; Consiglio, G.; Grasso, G.; Satriano, C.; Forte, G. pH sensitive functionalized graphene oxide as a carrier for delivering Gemcitabine: A computational approach. *Comput. Theor. Chem.* **2016**, *1096*, 1–6. [[CrossRef](#)]
125. Ghazanfari, A.; Marasini, S.; Miao, X.; Park, J.A.; Jung, K.-H.; Ahmad, M.Y.; Yue, H.; Ho, S.L.; Liu, S.; Jang, Y.J. Synthesis, characterization, and X-ray attenuation properties of polyacrylic acid-coated ultrasmall heavy metal oxide (Bi_2O_3 , Yb_2O_3 , NaTaO_3 , Dy_2O_3 , and Gd_2O_3) nanoparticles as potential CT contrast agents. *Colloids Surf. A Physicochem. Eng. Asp.* **2019**, *576*, 73–81. [[CrossRef](#)]
126. Jia, X.; Yin, J.; He, D.; He, X.; Wang, K.; Chen, M.; Li, Y. Polyacrylic acid modified upconversion nanoparticles for simultaneous pH-triggered drug delivery and release imaging. *J. Biomed. Nanotechnol.* **2013**, *9*, 2063–2072. [[CrossRef](#)]
127. Ma, Y.; Ji, Y.; You, M.; Wang, S.; Dong, Y.; Jin, G.; Lin, M.; Wang, Q.; Li, A.; Zhang, X. Labeling and long-term tracking of bone marrow mesenchymal stem cells in vitro using $\text{NaYF}_4: \text{Yb}^{3+}, \text{Er}^{3+}$ upconversion nanoparticles. *Acta Biomater.* **2016**, *42*, 199–208. [[CrossRef](#)] [[PubMed](#)]
128. Ma, Y.; Wang, X.; Chen, H.; Miao, Z.; He, G.; Zhou, J.; Zha, Z. Polyacrylic acid functionalized Co^{0} . ^{85}Se nanoparticles: An ultrasmall pH-responsive nanocarrier for synergistic photothermal-chemo treatment of cancer. *ACS Biomater. Sci. Eng.* **2018**, *4*, 547–557. [[CrossRef](#)] [[PubMed](#)]
129. Shi, H.; Li, L.; Zhang, L.; Wang, T.; Wang, C.; Zhu, D.; Su, Z. Designed preparation of polyacrylic acid/calcium carbonate nanoparticles with high doxorubicin payload for liver cancer chemotherapy. *CrystEngComm* **2015**, *17*, 4768–4773. [[CrossRef](#)]
130. Zhang, K.; Zhuang, Y.; Li, J.; Liu, X.; He, S. Poly (Acrylic Acid)-Modified MoS_2 Nanoparticle-Based Transdermal Delivery of Atenolol. *Int. J. Nanomed.* **2020**, *15*, 5517. [[CrossRef](#)] [[PubMed](#)]
131. Xu, Y.; Lin, Y.; Zhuang, L.; Lin, J.; Lv, J.; Huang, Q.; Sun, J. Bleomycin loaded magnetite nanoparticles functionalized by polyacrylic acid as a new antitumoral drug delivery system. *BioMed Res. Int.* **2013**, *2013*, 462589. [[CrossRef](#)]
132. Cui, Y.; Zhang, C.; Luo, R.; Liu, H.; Zhang, Z.; Xu, T.; Zhang, Y.; Wang, D. Noninvasive monitoring of early antiangiogenic therapy response in human nasopharyngeal carcinoma xenograft model using MRI with RGD-conjugated ultrasmall superparamagnetic iron oxide nanoparticles. *Int. J. Nanomed.* **2016**, *11*, 5671. [[CrossRef](#)]
133. Giraldo-Villegas, M.; Urquijo, J.; Arnache-Olmos, O.L.; Rojas-López, M. Polyacrylic acid-coated iron oxide nanoparticles could be a useful tool for tracking inflammatory monocytes. *Future Sci. OA* **2019**, *5*, FSO423. [[CrossRef](#)]
134. Padwal, P.; Bandyopadhyaya, R.; Mehra, S. Polyacrylic acid-coated iron oxide nanoparticles for targeting drug resistance in mycobacteria. *Langmuir* **2014**, *30*, 15266–15276. [[CrossRef](#)]
135. Lojk, J.; Bregar, V.B.; Rajh, M.; Miš, K.; Kreft, M.E.; Pirkmajer, S.; Veranič, P.; Pavlin, M. Cell type-specific response to high intracellular loading of polyacrylic acid-coated magnetic nanoparticles. *Int. J. Nanomed.* **2015**, *10*, 1449.
136. Bian, R.; Wang, T.; Zhang, L.; Li, L.; Wang, C. A combination of tri-modal cancer imaging and in vivo drug delivery by metal-organic framework based composite nanoparticles. *Biomater. Sci.* **2015**, *3*, 1270–1278. [[CrossRef](#)]
137. Kang, X.J.; Dai, Y.L.; Ma, P.A.; Yang, D.M.; Li, C.X.; Hou, Z.Y.; Cheng, Z.Y.; Lin, J. Poly (acrylic acid)-modified Fe_3O_4 microspheres for magnetic-targeted and pH-triggered anticancer drug delivery. *Chem. Eur. J.* **2012**, *18*, 15676–15682. [[CrossRef](#)] [[PubMed](#)]
138. Chen, L.; Li, L.; Zhang, L.; Xing, S.; Wang, T.; Wang, Y.A.; Wang, C.; Su, Z. Designed fabrication of unique eccentric mesoporous silica nanocluster-based core-shell nanostructures for pH-responsive drug delivery. *ACS Appl. Mater. Interfaces* **2013**, *5*, 7282–7290. [[CrossRef](#)]
139. Esfahanian, M.; Ghasemzadeh, M.A.; Razavian, S.M.H. Synthesis, identification and application of the novel metal-organic framework $\text{Fe}_3\text{O}_4@ \text{PAA} @ \text{ZIF-8}$ for the drug delivery of ciprofloxacin and investigation of antibacterial activity. *Artif. Cells Nanomed. Biotechnol.* **2019**, *47*, 2024–2030. [[CrossRef](#)] [[PubMed](#)]
140. Chen, Y.; Nan, J.; Lu, Y.; Wang, C.; Chu, F.; Gu, Z. Hybrid Fe_3O_4 -poly (acrylic acid) nanogels for theranostic cancer treatment. *J. Biomed. Nanotechnol.* **2015**, *11*, 771–779. [[CrossRef](#)] [[PubMed](#)]
141. Moscoso-Londoño, O.; Gonzalez, J.S.; Muraca, D.; Hoppe, C.E.; Alvarez, V.A.; López-Quintela, A.; Socolovsky, L.M.; Pirota, K. Structural and magnetic behavior of ferrogels obtained by freezing thawing of polyvinyl alcohol/poly (acrylic acid)(PAA)-coated iron oxide nanoparticles. *Eur. Polym. J.* **2013**, *49*, 279–289. [[CrossRef](#)]
142. Amini-Fazl, M.S.; Mohammadi, R.; Kheiri, K. 5-Fluorouracil loaded chitosan/polyacrylic acid/ Fe_3O_4 magnetic nanocomposite hydrogel as a potential anticancer drug delivery system. *Int. J. Biol. Macromol.* **2019**, *132*, 506–513. [[CrossRef](#)]
143. Iversen, N.K.; Frische, S.; Thomsen, K.; Laustsen, C.; Pedersen, M.; Hansen, P.B.; Bie, P.; Fresnais, J.; Berret, J.-F.; Baatrup, E. Superparamagnetic iron oxide polyacrylic acid coated $\gamma\text{-Fe}_2\text{O}_3$ nanoparticles do not affect kidney function but cause acute effect on the cardiovascular function in healthy mice. *Toxicol. Appl. Pharmacol.* **2013**, *266*, 276–288. [[CrossRef](#)]
144. Surendra, M.K.; Annapoorani, S.; Ansar, E.B.; Varma, P.H.; Rao, M.R. Magnetic hyperthermia studies on water-soluble polyacrylic acid-coated cobalt ferrite nanoparticles. *J. Nanopart. Res.* **2014**, *16*, 2773. [[CrossRef](#)]
145. Chandekar, K.V.; Shkir, M.; Alshahrani, T.; Ibrahim, E.H.; Kilany, M.; Ahmad, Z.; Manthrammel, M.A.; AlFaify, S.; Kateb, B.; Kaushik, A. One-spot fabrication and in-vivo toxicity evaluation of core-shell magnetic nanoparticles. *Mater. Sci. Eng. C* **2021**, *122*, 111898. [[CrossRef](#)]
146. Irfan, M.; Dogan, N.; Bingolbali, A.; Aliew, F. Synthesis and characterization of NiFe_2O_4 magnetic nanoparticles with different coating materials for magnetic particle imaging (MPI). *J. Magn. Magn. Mater.* **2021**, *537*, 168150. [[CrossRef](#)]

147. Foroushani, M.S.; Zahmatkeshan, A.; Arkaban, H.; Shervedani, R.K.; Kefayat, A. A drug delivery system based on nanocomposites constructed from metal-organic frameworks and Mn_3O_4 nanoparticles: Preparation and physicochemical characterization for BT-474 and MCF-7 cancer cells. *Colloids Surf. B Biointerfaces* **2021**, *202*, 111712. [[CrossRef](#)] [[PubMed](#)]
148. Talusan, T.J.E.; Baltazar, M.C.P.; Usman, K.A.S.; Payawan, L.M., Jr. Synthesis of glucose-sensitive microcapsules via layer-by-layer assembly for controlled insulin release applications. *Appl. Mech. Mater.* **2017**, *863*, 84–88. [[CrossRef](#)]
149. Huang, J.; Huang, Y.; Xue, Z.; Zeng, S. Tumor microenvironment responsive hollow mesoporous $Co_9S_8@MnO_2$ -ICG/DOX intelligent nanoplatform for synergistically enhanced tumor multimodal therapy. *Biomaterials* **2020**, *262*, 120346. [[CrossRef](#)] [[PubMed](#)]
150. Jian-Hua, L.; Lei, W.; ZHANG, T.-Q.; Jian-Qiu, W.; Xue, G.; Feng-Zhi, C.; ZHENG, J.-J.; Bo, L.; Zhan, S. Facile Synthesis of Biocompatible Fe_3O_4 -Based Nanoparticles for pH-Responsive Dual-Model Magnetic Resonance Imaging-Guided Tumour Eradication by Photothermal Therapy. *Chin. J. Anal. Chem.* **2019**, *47*, 678–685.
151. Zhang, Q.; Wang, W.; Zhang, M.; Wu, F.; Zheng, T.; Sheng, B.; Liu, Y.; Shen, J.; Zhou, N.; Sun, Y. A theranostic nanocomposite with integrated black phosphorus nanosheet, $Fe_3O_4@MnO_2$ -doped upconversion nanoparticles and chlorin for simultaneous multimodal imaging, highly efficient photodynamic and photothermal therapy. *Chem. Eng. J.* **2020**, *391*, 123525. [[CrossRef](#)]
152. Javakhshvili, I.; Hvilsted, S. Gold Nanoparticles Protected with Thiol-Derivatized Amphiphilic Poly (ϵ -caprolactone)-b-poly (acrylic acid). *Biomacromolecules* **2009**, *10*, 74–81. [[CrossRef](#)]
153. Lin, I.-C.; Liang, M.; Liu, T.-Y.; Ziora, Z.M.; Monteiro, M.J.; Toth, I. Interaction of densely polymer-coated gold nanoparticles with epithelial Caco-2 monolayers. *Biomacromolecules* **2011**, *12*, 1339–1348. [[CrossRef](#)]
154. Mahmoodzadeh, F.; Abbasian, M.; Jaymand, M.; Salehi, R.; Bagherzadeh-Khajehmarjan, E. A novel gold-based stimuli-responsive theranostic nanomedicine for chemo-photothermal therapy of solid tumors. *Mater. Sci. Eng. C* **2018**, *93*, 880–889. [[CrossRef](#)]
155. Deng, Z.J.; Liang, M.; Monteiro, M.; Toth, I.; Minchin, R.F. Nanoparticle-induced unfolding of fibrinogen promotes Mac-1 receptor activation and inflammation. *Nat. Nanotechnol.* **2011**, *6*, 39–44. [[CrossRef](#)]
156. Bardajee, G.R.; Mizani, F.; Hosseini, S.S. pH sensitive release of doxorubicin anticancer drug from gold nanocomposite hydrogel based on poly (acrylic acid) grafted onto salep biopolymer. *J. Polym. Res.* **2017**, *24*, 1–13. [[CrossRef](#)]
157. Khan, I.M.; Niazi, S.; Yu, Y.; Pasha, I.; Yue, L.; Mohsin, A.; Shoaib, M.; Iqbal, M.W.; Khaliq, A.; Wang, Z. Fabrication of PAA coated green-emitting AuNCs for construction of label-free FRET assembly for specific recognition of T-2 toxin. *Sens. Actuators B Chem.* **2020**, *321*, 128470. [[CrossRef](#)]
158. Wang, L.; Pei, J.; Cong, Z.; Zou, Y.; Sun, T.; Davitt, F.; Garcia-Gil, A.; Holmes, J.D.; O'Driscoll, C.M.; Rahme, K. Development of anisamide-targeted PEGylated gold nanorods to deliver epirubicin for chemo-photothermal therapy in tumor-bearing mice. *Int. J. Nanomed.* **2019**, *14*, 1817. [[CrossRef](#)] [[PubMed](#)]
159. Wang, Q.; Jin, X.Q.; Sun, J.H.; Bai, S.Y.; Wu, X. PAA-grafted surface and fractal feature of dense nanosilica spheres for ibuprofen delivery. *Mater. Chem. Phys.* **2017**, *195*, 213–223. [[CrossRef](#)]
160. Tian, F.; Kaňka, J.; Yang, F.; Min, J.; Hammond, P.T. Role of silica nanoparticles in monitoring and prolonging release of drug-eluting polyelectrolyte coatings using long-period fiber grating platform. *Sens. Actuators B Chem.* **2017**, *252*, 831–839. [[CrossRef](#)]
161. Runowski, M.; Lis, S. Synthesis, surface modification/decoration of luminescent-magnetic core/shell nanomaterials, based on the lanthanide doped fluorides ($Fe_3O_4/SiO_2/NH_2/PAA/LnF_3$). *J. Lumin.* **2016**, *170*, 484–490. [[CrossRef](#)]
162. Liu, D.; Li, Z.; Li, G.; Wang, F.; Wang, W. Synthesis of hollow α - Fe_2O_3 -silica composites templated by poly (acrylic acid) colloidal aggregates. *J. Coat. Technol. Res.* **2014**, *11*, 595–600. [[CrossRef](#)]
163. Jin, X.; Wang, Q.; Sun, J.; Panezai, H.; Bai, S.; Wu, X. Dual (pH-and temperature-) stimuli responsive nanocarrier with bimodal mesoporous silica nanoparticles core and copolymer shell for controlled ibuprofen-releasing: Fractal feature and diffusion mechanism. *Microporous Mesoporous Mater.* **2017**, *254*, 77–85. [[CrossRef](#)]
164. Cabana, S.; Lecona-Vargas, C.S.; Meléndez-Ortiz, H.I.; Contreras-García, A.; Barbosa, S.; Taboada, P.; Magarinos, B.; Bucio, E.; Concheiro, A.; Alvarez-Lorenzo, C. Silicone rubber films functionalized with poly (acrylic acid) nanobrushes for immobilization of gold nanoparticles and photothermal therapy. *J. Drug Deliv. Sci. Technol.* **2017**, *42*, 245–254. [[CrossRef](#)]
165. Han, J.-H.; Jung, S.-W. Encapsulating metal-organic frameworks (MOFs) with calcium phosphate (CaP) for pH-responsive drug delivery. *Korea Ind. Chem. Soc.* **2019**, *2019*, 194.
166. Wu, L.; Hu, Y.; Tang, P.; Wang, H.; Bin, Y. High stretchable, pH-sensitive and self-adhesive rGO/CMCNa/PAA composite conductive hydrogel with good strain-sensing performance. *Compos. Commun.* **2021**, *24*, 100669. [[CrossRef](#)]
167. Zhu, Q.; Liu, L.; Wang, R.; Zhou, X. A split aptamer (SPA)-based sandwich-type biosensor for facile and rapid detection of streptomycin. *J. Hazard. Mater.* **2021**, *403*, 123941. [[CrossRef](#)]
168. Ortega, V.A.; Cameron, M.S.; Stafford, J.L.; Goss, G.G.; Donald, J.A.; Schultz, A.G. Polyacrylic acid coated nanoparticles elicit endothelial cell apoptosis and diminish vascular relaxation in ex vivo perfused iliac arteries of the cane toad (*Rhinella marina*). *Environ. Sci. Nano* **2020**, *7*, 1912–1926. [[CrossRef](#)]
169. Morita, K.; Suzuki, T.; Nishimura, Y.; Matsumoto, K.; Numako, C.; Sato, K.; Nakayama, M.; Sasaki, R.; Ogino, C.; Kondo, A. In vivo tissue distribution and safety of polyacrylic acid-modified titanium peroxide nanoparticles as novel radiosensitizers. *J. Biosci. Bioeng.* **2018**, *126*, 119–125. [[CrossRef](#)] [[PubMed](#)]
170. Hanafy, N.; El-Kemary, M.; Leporatti, S. Reduction diameter of $CaCO_3$ crystals by using poly acrylic acid might improve cellular uptake of encapsulated curcumin in breast cancer. *J. Nanomed. Res* **2018**, *7*, 235–239.

171. Baldim, V.; Yadav, N.; Bia, N.; Graillot, A.; Loubat, C.; Singh, S.; Karakoti, A.S.; Berret, J.-F. Polymer-coated cerium oxide nanoparticles as oxidoreductase-like catalysts. *ACS Appl. Mater. Interfaces* **2020**, *12*, 42056–42066. [[CrossRef](#)] [[PubMed](#)]
172. Chu, Y.-M.; Nazir, U.; Sohail, M.; Selim, M.M.; Lee, J.-R. Enhancement in thermal energy and solute particles using hybrid nanoparticles by engaging activation energy and chemical reaction over a parabolic surface via finite element approach. *Fractal Fract.* **2021**, *5*, 119. [[CrossRef](#)]
173. Li, B.; Li, C.; Zhang, Y.; Wang, Y.; Jia, D.; Yang, M.; Zhang, N.; Wu, Q.; Han, Z.; Sun, K. Heat transfer performance of MQL grinding with different nanofluids for Ni-based alloys using vegetable oil. *J. Clean. Prod.* **2017**, *154*, 1–11. [[CrossRef](#)]
174. Wang, Y.; Li, C.; Zhang, Y.; Li, B.; Yang, M.; Zhang, X.; Guo, S.; Liu, G. Experimental evaluation of the lubrication properties of the wheel/workpiece interface in MQL grinding with different nanofluids. *Tribol. Int.* **2016**, *99*, 198–210. [[CrossRef](#)]
175. Yang, Y.; Gong, Y.; Li, C.; Wen, X.; Sun, J. Mechanical performance of 316 L stainless steel by hybrid directed energy deposition and thermal milling process. *J. Mater. Process. Technol.* **2021**, *291*, 117023. [[CrossRef](#)]
176. Zhang, Z.; Cui, F.; Cao, C.; Wang, Q.; Zou, Q. Single-cell RNA analysis reveals the potential risk of organ-specific cell types vulnerable to SARS-CoV-2 infections. *Comput. Biol. Med.* **2022**, *140*, 105092. [[CrossRef](#)]
177. Zha, T.-H.; Castillo, O.; Jahanshahi, H.; Yusuf, A.; Alassafi, M.O.; Alsaadi, F.E.; Chu, Y.-M. A fuzzy-based strategy to suppress the novel coronavirus (2019-NCOV) massive outbreak. *Appl. Comput. Math.* **2021**, *20*, 160–176.
178. Nazeer, M.; Hussain, F.; Khan, M.I.; El-Zahar, E.R.; Chu, Y.-M.; Malik, M. Theoretical study of MHD electro-osmotically flow of third-grade fluid in micro channel. *Appl. Math. Comput.* **2022**, *420*, 126868. [[CrossRef](#)]
179. Zhao, T.H.; Khan, M.I.; Chu, Y.M. Artificial neural networking (ANN) analysis for heat and entropy generation in flow of non-Newtonian fluid between two rotating disks. *Math. Methods Appl. Sci.* **2021**, *1*, 1–14. [[CrossRef](#)]
180. Wang, F.; Khan, M.N.; Ahmad, I.; Ahmad, H.; Abu-Zinadah, H.; Chu, Y.-M. Numerical solution of traveling waves in chemical kinetics: Time-fractional fishers equations. *Fractals* **2022**, *1*, 2240051. [[CrossRef](#)]
181. Song, Y.-Q.; Zhao, T.-H.; Chu, Y.-M.; Zhang, X.-H. Optimal evaluation of a Toader-type mean by power mean. *J. Inequalities Appl.* **2015**, *2015*, 408. [[CrossRef](#)]
182. Chu, Y.-M.; Shankaralingappa, B.; Gireesha, B.; Alzahrani, F.; Khan, M.I.; Khan, S.U. Combined impact of Cattaneo-Christov double diffusion and radiative heat flux on bio-convective flow of Maxwell liquid configured by a stretched nano-material surface. *Appl. Math. Comput.* **2022**, *419*, 126883. [[CrossRef](#)]
183. Guo, S.; Li, C.; Zhang, Y.; Wang, Y.; Li, B.; Yang, M.; Zhang, X.; Liu, G. Experimental evaluation of the lubrication performance of mixtures of castor oil with other vegetable oils in MQL grinding of nickel-based alloy. *J. Clean. Prod.* **2017**, *140*, 1060–1076. [[CrossRef](#)]
184. Lai, W.-F. Development of Hydrogels with Self-Healing Properties for Delivery of Bioactive Agents. *Mol. Pharm.* **2021**, *18*, 1833–1841. [[CrossRef](#)]
185. Liu, X.; Chang, M.; He, B.; Meng, L.; Wang, X.; Sun, R.; Ren, J.; Kong, F. A one-pot strategy for preparation of high-strength carboxymethyl xylan-g-poly (acrylic acid) hydrogels with shape memory property. *J. Colloid Interface Sci.* **2019**, *538*, 507–518. [[CrossRef](#)]
186. Posha, B.; Sandhyarani, N.J. Highly sensitive endotoxin detection using a gold nanoparticle loaded layered molybdenum disulfide-polyacrylic acid nanocomposite. *Analyst* **2020**, *145*, 3939–3947. [[CrossRef](#)]
187. Zhang, Z.; Zhang, S.; He, L.; Peng, D.; Yan, F.; Wang, M.; Zhao, J.; Zhang, H.; Fang, S. Feasible electrochemical biosensor based on plasma polymerization-assisted composite of polyacrylic acid and hollow TiO₂ spheres for sensitively detecting lysozyme. *Biosens. Bioelectron.* **2015**, *74*, 384–390. [[CrossRef](#)] [[PubMed](#)]
188. Rong, Q.; Feng, F.; Ma, Z. Metal ions doped chitosan-poly (acrylic acid) nanospheres: Synthesis and their application in simultaneously electrochemical detection of four markers of pancreatic cancer. *Biosens. Bioelectron.* **2016**, *75*, 148–154. [[CrossRef](#)] [[PubMed](#)]
189. Ghimire, A.; Zore, O.V.; Thilakarathne, V.K.; Briand, V.A.; Lenehan, P.J.; Lei, Y.; Kasi, R.M.; Kumar, C.V. “Stable-on-the-table” biosensors: Hemoglobin-poly (acrylic acid) nanogel bioelectrodes with high thermal stability and enhanced electroactivity. *Sensors* **2015**, *15*, 23868–23885. [[CrossRef](#)] [[PubMed](#)]
190. Johnson, K.C.; Mendez, F.; Serpe, M.J. Detecting solution pH changes using poly (N-isopropylacrylamide)-co-acrylic acid microgel-based etalon modified quartz crystal microbalances. *Anal. Chim. Acta* **2012**, *739*, 83–88. [[CrossRef](#)]
191. Akkahat, P.; Mekboonsonglar, W.; Kiatkamjornwong, S.; Hoven, V.P. Surface-grafted poly (acrylic acid) brushes as a precursor layer for biosensing applications: Effect of graft density and swellability on the detection efficiency. *Langmuir* **2012**, *28*, 5302–5311. [[CrossRef](#)]
192. Akkahat, P.; Hoven, V.P. Introducing surface-tethered poly (acrylic acid) brushes as 3D functional thin film for biosensing applications. *Colloids Surf. B Biointerfaces* **2011**, *86*, 198–205. [[CrossRef](#)]
193. Yin, Z.; Cui, R.; Liu, Y.; Jiang, L.; Zhu, J.-J. Ultrasensitive electrochemical immunoassay based on cadmium ion-functionalized PSA@PAA nanospheres. *Biosens. Bioelectron.* **2010**, *25*, 1319–1324. [[CrossRef](#)]
194. Liu, A.; Watanabe, T.; Honma, I.; Wang, J.; Zhou, H. Effect of solution pH and ionic strength on the stability of poly (acrylic acid)-encapsulated multiwalled carbon nanotubes aqueous dispersion and its application for NADH sensor. *Biosens. Bioelectron.* **2006**, *22*, 694–699. [[CrossRef](#)]
195. Rather, A.; Wani, G.M.; Robbani, I. Multidetector-Row Computed Tomography and Colour Doppler Imaging in the Evaluation of Patients with Extrahepatic Portal Hypertension: A Prospective Study. *Int. J. Sci. Res. Dent. Med. Sci.* **2021**, *3*, 86–93.

196. Zhao, Y.; Wu, R.; Yu, H.; Li, J.; Liu, L.; Wang, S.; Chen, X.; Chan, T.-W.D. Magnetic solid-phase extraction of sulfonamide antibiotics in water and animal-derived food samples using core-shell magnetite and molybdenum disulfide nanocomposite adsorbent. *J. Chromatogr. A* **2020**, *1610*, 460543. [[CrossRef](#)]
197. Nuñez, N.O.; Cussó, F.; Cantelar, E.; Martín-Gracia, B.; de la Fuente, J.M.; Corral, A.; Balcerzyk, M.; Ocaña, M. Bimodal Nd-doped LuVO₄ nanoprobe functionalized with polyacrylic acid for x-ray computed tomography and NIR luminescent imaging. *Nanomaterials* **2020**, *10*, 149. [[CrossRef](#)] [[PubMed](#)]
198. Goma, O.M.; Okasha, A.; Hosni, H.M.; Ali, A.E.-H. Biocompatible Water Soluble Polyacrylic Acid Coated CdSe/Cu Quantum Dot Conjugates for Biomolecule Detection. *J. Fluoresc.* **2018**, *28*, 41–49. [[CrossRef](#)] [[PubMed](#)]
199. Nuñez, N.O.; García, M.; García-Sevillano, J.; Rivera-Fernández, S.; de la Fuente, J.M.; Ocaña, M. One-Step Synthesis and Polyacrylic Acid Functionalization of Multifunctional Europium-Doped NaGdF₄ Nanoparticles with Selected Size for Optical and MRI Imaging. *Eur. J. Inorg. Chem.* **2014**, *2014*, 6075–6084. [[CrossRef](#)]
200. Escudero, A.; Carrillo-Carrión, C.; Zyuzin, M.V.; Ashraf, S.; Hartmann, R.; Núñez, N.O.; Ocaña, M.; Parak, W.J. Synthesis and functionalization of monodisperse near-ultraviolet and visible excitable multifunctional Eu³⁺, Bi³⁺: REVO₄ nanophosphors for bioimaging and biosensing applications. *Nanoscale* **2016**, *8*, 12221–12236. [[CrossRef](#)] [[PubMed](#)]
201. Xue, Z.; Zeng, S.; Hao, J. Non-invasive through-skull brain vascular imaging and small tumor diagnosis based on NIR-II emissive lanthanide nanoprobe beyond 1500 nm. *Biomaterials* **2018**, *171*, 153–163. [[CrossRef](#)]
202. Sargazi, G.; Ebrahimi, A.K.; Afzali, D.; Badoei-dalfard, A.; Malekabadi, S.; Karami, Z. Fabrication of PVA/ZnO fibrous composite polymer as a novel sorbent for arsenic removal: Design and a systematic study. *Polym. Bull.* **2019**, *76*, 5661–5682. [[CrossRef](#)]
203. Tang, L.; Zhang, Y.; Li, C.; Zhou, Z.; Nie, X.; Chen, Y.; Cao, H.; Liu, B.; Zhang, N.; Said, Z. Biological stability of water-based cutting fluids: Progress and application. *Chin. J. Mech. Eng.* **2022**, *35*, 3. [[CrossRef](#)]
204. Zhang, Z.; Sui, M.; Li, C.; Zhou, Z.; Liu, B.; Chen, Y.; Said, Z.; Debnath, S.; Sharma, S. Residual stress of MoS₂ nano-lubricant grinding cemented carbide. *Int. J. Adv. Manuf. Technol.* **2021**, *1*, 1–15. [[CrossRef](#)]
205. Nnaemeka, O.; Phyllis, N.; Chinaza, O. The Use of Herbal Medicines in Pregnancy: A Cross-sectional Analytic Study. *Int. J. Sci. Res. Dent. Med. Sci.* **2021**, *3*, 66–72.
206. Shangloo, P.; Gupte, B.; Syed, M. Histopathological Effect of Arsenic in Drinking Water on Liver and Kidney of Albino Rat: A Light Microscopic Study. *Int. J. Sci. Res. Dent. Med. Sci.* **2021**, *3*, 166–170.
207. Mohammadi, L.; Pal, K.; Bilal, M.; Rahdar, A.; Fytianos, G.; Kyzas, G.Z. Green nanoparticles to treat patients with Malaria disease: An overview. *J. Mol. Struct.* **2021**, *1229*, 129857. [[CrossRef](#)]
208. Zong, X.; Xiao, X.; Shen, B.; Jiang, Q.; Wang, H.; Lu, Z.; Wang, F.; Jin, M.; Min, J.; Wang, F. The N⁶-methyladenosine RNA-binding protein YTHDF1 modulates the translation of TRAF6 to mediate the intestinal immune response. *Nucleic Acids Res.* **2021**, *49*, 5537–5552. [[CrossRef](#)] [[PubMed](#)]
209. Islam, M.; Sultana, G.; Khan, R.; Islam, A.; Mahmud, H.; Raihan, S. Study on Mitochondrial ATPase6 Gene Polymorphisms as a Genetic Risk Factor for Breast Cancer in Bangladeshi Women. *Int. J. Sci. Res. Dent. Med. Sci.* **2021**, *3*, 18–22.
210. Jamali, S.; Kasraei, E.; Rezazadeh Kalashami, A.; Barri Dizaj, M. Strategy for Treating the Gastric Cancer: A Systematic Review and Meta-analysis. *Int. J. Sci. Res. Dent. Med. Sci.* **2020**, *2*, 6–11.
211. Jamali, S.; Marcella, C.; Prakash, P.; Moradkhani, A.; Kasraei, E. Prevalence of Malignancy and Chronic Obstructive Pulmonary Disease among Patients with COVID-19: A Systematic Review and Meta-analysis. *Int. J. Sci. Res. Dent. Med. Sci.* **2020**, *2*, 52–58.
212. Dinita Devi, N.; Chyrmang, D.; Baidya, K.; Devi, Y.S. Askin Tumor: A Case Report of a Rare Tumor. *Int. J. Sci. Res. Dent. Med. Sci.* **2021**, *3*, 153–155.
213. Hamidian, K.; Sarani, M.; Sheikhi, E.; Khatami, M. Cytotoxicity evaluation of green synthesized ZnO and Ag-doped ZnO nanoparticles on brain glioblastoma cells. *J. Mol. Struct.* **2022**, *1251*, 131962. [[CrossRef](#)]
214. Zhang, K.; Zhang, Y.; Li, Y.; Iqbal, Z.; Yu, L.; Liu, J.; Wang, H.; He, P. The thermal/pH-sensitive drug delivery system encapsulated by PAA based on hollow hybrid nanospheres with two silicon source. *J. Biomater. Sci. Polym. Ed.* **2021**, *32*, 695–713. [[CrossRef](#)]
215. Bagheri, N.; Lakouraj, M.M.; Nabavi, S.R.; Tashakkorian, H.; Mohseni, M. Synthesis of bioactive polyaniline-b-polyacrylic acid copolymer nanofibrils as an effective antibacterial and anticancer agent in cancer therapy, especially for HT29 treatment. *RSC Adv. RSC Adv.* **2020**, *10*, 25290–25304. [[CrossRef](#)]
216. Li, Y.; Wan, J.; Wang, F.; Guo, J.; Wang, C. Effect of increasing liver blood flow on nanodrug clearance by the liver for enhanced antitumor therapy. *Biomater. Sci.* **2019**, *7*, 1507–1515. [[CrossRef](#)]
217. Reddy, B.N.; Rauta, P.R.; Lakshmi, V.V.; Sreenivasa, S. Development, formulation, and evaluation of sodium alginate-g-poly (acryl amide-co-acrylic acid/cloiste-30b)/agnps hydrogel composites and their applications in paclitaxel drug delivery and anticancer activity. *Int. J. Appl. Pharm.* **2018**, *10*, 141–150.
218. Tan, S.; Wang, G. Redox-responsive and pH-sensitive nanoparticles enhanced stability and anticancer ability of erlotinib to treat lung cancer in vivo. *Drug Des. Dev. Ther.* **2017**, *11*, 3519. [[CrossRef](#)] [[PubMed](#)]
219. Wang, Y.; Zhang, X.-Y.; Luo, Y.-L.; Xu, F.; Chen, Y.-S.; Su, Y.-Y. Dual stimuli-responsive Fe₃O₄ graft poly (acrylic acid)-block-poly (2-methacryloyloxyethyl ferrocenecarboxylate) copolymer micelles: Surface RAFT synthesis, self-assembly and drug release applications. *J. Nanobiotechnol.* **2017**, *15*, 76. [[CrossRef](#)] [[PubMed](#)]
220. Tian, B.; Liu, S.; Wu, S.; Lu, W.; Wang, D.; Jin, L.; Hu, B.; Li, K.; Wang, Z.; Quan, Z.; et al. pH-responsive poly (acrylic acid)-gated mesoporous silica and its application in oral colon targeted drug delivery for doxorubicin. *Colloids Surf. B Biointerfaces* **2017**, *154*, 287–296. [[CrossRef](#)] [[PubMed](#)]

221. Hao, N.; Li, L.; Tang, F. Shape matters when engineering mesoporous silica-based nanomedicines. *Biomater. Sci.* **2016**, *4*, 575–591. [[CrossRef](#)]
222. Yuan, S.; Chen, J.; Sheng, J.; Hu, Y.; Jiang, Z. Paclitaxel-Loaded β -Cyclodextrin-Modified Poly (Acrylic Acid) Nanoparticles through Multivalent Inclusion for Anticancer Therapy. *Macromol. Biosci.* **2016**, *16*, 341–349. [[CrossRef](#)]
223. Chiang, C.S.; Tseng, Y.H.; Liao, B.J.; Chen, S.Y. Magnetically targeted nanocapsules for PAA-cisplatin-conjugated cores in PVA/SPIO shells via surfactant-free emulsion for reduced nephrotoxicity and enhanced lung cancer therapy. *Adv. Healthc. Mater.* **2015**, *4*, 1066–1075. [[CrossRef](#)]
224. Lee, K.D.; Jeong, Y.-I.; Da Hye Kim, G.-T.L.; Choi, K.-C. Cisplatin-incorporated nanoparticles of poly (acrylic acid-co-methyl methacrylate) copolymer. *Int. J. Nanomed.* **2013**, *8*, 2835.
225. Zhao, Y.; Liu, Y.; Wang, Y.; Xu, B.; Zhang, S.; Liu, J.; Zhang, T.; Jin, L.; Song, S.; Zhang, H. Rapidly clearable MnCo_2O_4 @PAA as novel nanotheranostic agents for T_1/T_2 bimodal MRI imaging-guided photothermal therapy. *Nanoscale* **2021**, *13*, 16251–16257. [[CrossRef](#)]
226. Li, D.; Bao, A.; Chen, X.; Li, S.; Wang, T.; Zhang, L.; Ji, J.; Li, Q.; Wang, C.; Gao, Y.; et al. Prussian Blue@ Polyacrylic Acid/ Au Aggregate Janus Nanoparticles for CT Imaging-guided Chemotherapy and Enhanced Photothermal Therapy. *Adv. Ther.* **2020**, *3*, 2000091. [[CrossRef](#)]
227. Zhao, S.; Tian, R.; Shao, B.; Feng, Y.; Yuan, S.; Dong, L.; Zhang, L.; Wang, Z.; You, H. One-pot synthesis of Ln 3+-doped porous BiF 3@PAA nanospheres for temperature sensing and pH-responsive drug delivery guided by CT imaging. *Nanoscale* **2020**, *12*, 695–702. [[CrossRef](#)] [[PubMed](#)]
228. Li, L.; Zhang, L.; Wang, T.; Wu, X.; Ren, H.; Wang, C.; Su, Z. Facile and Scalable Synthesis of Novel Spherical Au Nanocluster Assemblies@ Polyacrylic Acid/Calcium Phosphate Nanoparticles for Dual-Modal Imaging-Guided Cancer Chemotherapy. *Small* **2015**, *11*, 3162–3173. [[CrossRef](#)]
229. Huang, H.-Y.; Hu, S.-H.; Hung, S.-Y.; Chiang, C.-S.; Liu, H.-L.; Chiu, T.-L.; Lai, H.-Y.; Chen, Y.-Y.; Chen, S.-Y. SPIO nanoparticle-stabilized PAA-F127 thermosensitive nanobubbles with MR/US dual-modality imaging and HIFU-triggered drug release for magnetically guided in vivo tumor therapy. *J. Control. Release* **2013**, *172*, 118–127. [[CrossRef](#)] [[PubMed](#)]
230. Hajikhani, M.; Emam Djomeh, Z.; Askari, G. Lycopene loaded polylactic acid (PLA) and PLA/copolymer electrospun nanofibers, synthesis, characterization, and control release. *J. Food Process. Preserv.* **2021**, *45*, e15055. [[CrossRef](#)]
231. Khajeh, H.G.; Sabzi, M.; Ramezani, S.; Jalili, A.A.; Ghorbani, M.J.C.; Physicochemical, S.A.; Aspects, E. Fabrication of a wound dressing mat based on Polyurethane/Polyacrylic acid containing Poloxamer for skin tissue engineering. *Colloids Surf. A Physicochem. Eng. Asp.* **2022**, *633*, 127891. [[CrossRef](#)]
232. Ghaffari-Bohlouli, P.; Zahedi, P.; Shahrousvand, M. Enhanced osteogenesis using poly (l-lactide-co-d, l-lactide)/poly (acrylic acid) nanofibrous scaffolds in presence of dexamethasone-loaded molecularly imprinted polymer nanoparticles. *Int. J. Biol. Macromol.* **2020**, *165*, 2363–2377. [[CrossRef](#)]
233. Cheng, Y.; Hu, Y.; Xu, M.; Qin, M.; Lan, W.; Huang, D.; Wei, Y.; Chen, W. High strength polyvinyl alcohol/polyacrylic acid (PVA/PAA) hydrogel fabricated by Cold-Drawn method for cartilage tissue substitutes. *J. Biomater. Sci. Polym. Ed.* **2020**, *31*, 1836–1851. [[CrossRef](#)] [[PubMed](#)]
234. Khan, M.U.A.; Haider, S.; Haider, A.; Abd Razak, S.I.; Kadir, M.R.A.; Shah, S.A.; Javed, A.; Shakir, I.; Al-Zahrani, A.A. Development of porous, antibacterial and biocompatible GO/n-HAp/bacterial cellulose/ β -glucan biocomposite scaffold for bone tissue engineering. *Arab. J. Chem.* **2021**, *14*, 102924. [[CrossRef](#)]
235. Nurkeeva, Z.S.; Khutoryanskiy, V.V.; Mun, G.A.; Sherbakova, M.V.; Ivaschenko, A.T.; Aitkhozhina, N.A. Polycomplexes of poly (acrylic acid) with streptomycin sulfate and their antibacterial activity. *Eur. J. Pharm. Biopharm.* **2004**, *57*, 245–249. [[CrossRef](#)]
236. Larsson, M.; Bergstrand, A.; Mesiah, L.; Van Vooren, C.; Larsson, A. Nanocomposites of polyacrylic acid nanogels and biodegradable polyhydroxybutyrate for bone regeneration and drug delivery. *J. Nanomater.* **2014**, *2014*, 371307. [[CrossRef](#)]
237. Ghorbaniazar, P.; Sepehrianazar, A.; Eskandani, M.; Nabi-Meibodi, M.; Kouhsoltani, M.; Hamishehkar, H. Preparation of poly acrylic acid-poly acrylamide composite nanogels by radiation technique. *Adv. Pharm. Bull.* **2015**, *5*, 269. [[CrossRef](#)] [[PubMed](#)]
238. Fathi, A.; Salehi, A. Antimicrobial resistance properties of Helicobacter pylori strains isolated from dental plaque and saliva samples. *Acad. J. Health Sci. Med. Balear* **2022**, *37*, 29–33.
239. Khamisi, N.; Fathi, A.; Yari, A. Antimicrobial resistance of Staphylococcus aureus isolated from dental plaques. *Acad. J. Health Sci. Med. Balear* **2022**, *37*, 136–140.
240. Ekwebene, O.; Nnamani, C.; Edeh, C.; Obidile, C.; Tyotswame, Y. Prevalence of Falciparum Malaria in Conjunction with Age, Gravidity, Abo Blood Group/Rhesus Factor, and Genotype Among Gravid Women in South-eastern Nigeria. *Int. J. Sci. Res. Dent. Med. Sci.* **2021**, *3*, 12–17.
241. Dilip, D.; Menon, A. Speciation, Detection of Virulence Factors and Antibiotic Susceptibility of Coagulase Negative Staphylococci. *Int. J. Sci. Res. Dent. Med. Sci.* **2021**, *3*, 122–132.
242. Sanaei, Z.; Azizi, A.; Rahimi, A. The Comparison of the Effect of Photodynamic Therapy Using two Photosensitizer Indocyanine Green and Methylene Blue on the Colony Count of Staphylococcus Aureus (In Vitro). *Int. J. Sci. Res. Dent. Med. Sci.* **2019**, *1*, 13–17.
243. Safari Kakroudi, M.; Rimaz, S.; Atrkar Roshan, Z.; Mobayen, M. The Frequency of Bacterial Colonization in Burn Wounds and Antibiogram pattern in Patients Hospitalized in the ICU of Velayat Burn and Reconstructive Surgery Center in Rasht City. *Int. J. Sci. Res. Dent. Med. Sci.* **2019**, *1*, 72–79.

244. Nazaripour, E.; Mosazadeh, F.; Rahimi, S.S.; Alijani, H.Q.; Isaei, E.; Borhani, F.; Irvani, S.; Ghasemi, M.; Akbarizadeh, M.R.; Azizi, E. Ferromagnetic nickel (II) oxide (NiO) nanoparticles: Biosynthesis, characterization and their antibacterial activities. *Rend. Lincei. Sci. Fis. E Nat.* **2022**, 1–8. [[CrossRef](#)]
245. Gratzl, G.; Paulik, C.; Hild, S.; Guggenbichler, J.P.; Lackner, M. Antimicrobial activity of poly (acrylic acid) block copolymers. *Mater. Sci. Eng. C* **2014**, *38*, 94–100. [[CrossRef](#)]
246. Brogden, K.A. Antimicrobial peptides: Pore formers or metabolic inhibitors in bacteria? *Nat. Rev. Microbiol.* **2005**, *3*, 238–250. [[CrossRef](#)]
247. Rivas, B.L.; Pereira, E.D.; Moreno-Villoslada, I. Water-soluble polymer–metal ion interactions. *Prog. Polym. Sci.* **2003**, *28*, 173–208. [[CrossRef](#)]
248. Sethy, P.K.; Mohapatra, P.; Patra, S.; Bharatiya, D.; Swain, S.K. Antimicrobial and barrier properties of polyacrylic acid/GO hybrid nanocomposites for packaging application. *Nano-Struct. Nano-Objects* **2021**, *26*, 100747. [[CrossRef](#)]
249. Gratzl, G.; Walkner, S.; Hild, S.; Hassel, A.W.; Weber, H.K.; Paulik, C. Mechanistic approaches on the antibacterial activity of poly (acrylic acid) copolymers. *Colloids Surf. B Biointerfaces* **2015**, *126*, 98–105. [[CrossRef](#)] [[PubMed](#)]
250. Chinthamreddy, A.; Koppula, S.; Kuruva, S.; Surya, S.M. 'Biopolymer-PAA and surfactant-CTAB assistant solvothermal synthesis of Zn-based MOFs: Design, characterization for removal of toxic dyes, copper and their biological activities. *Inorg. Chem. Commun.* **2021**, *133*, 108928. [[CrossRef](#)]
251. Shibraen, M.H.; Ibrahim, O.M.; Asad, R.A.; Yang, S.; El-Aassar, M.J.C.; Physicochemical, S.A.; Aspects, E. Interpenetration of metal cations into polyelectrolyte-multilayer-films via layer-by-layer assembly: Selective antibacterial functionality of cationic guar gum/polyacrylic acid-Ag⁺ nanofilm against resistant E. coli. *Colloids Surf. A Physicochem. Eng. Asp.* **2021**, *610*, 125921. [[CrossRef](#)]
252. Nie, L.; Chang, P.; Ji, C.; Zhang, F.; Zhou, Q.; Sun, M.; Sun, Y.; Politis, C.; Shavandi, A. Poly (acrylic acid) capped iron oxide nanoparticles via ligand exchange with antibacterial properties for biofilm applications. *Colloids Surf. B Biointerfaces* **2021**, *197*, 111385. [[CrossRef](#)]
253. Xu, X.; Wang, N.; Wu, M.; Wang, J.; Wang, D.; Chen, Z.; Xie, J.; Ding, C.; Li, J. Programmed antibacterial and mineralization therapy for dental caries based on zinc-substituted hydroxyapatite/alendronate-grafted polyacrylic acid hybrid material. *Colloids Surf. B Biointerfaces* **2020**, *194*, 111206. [[CrossRef](#)]
254. Sharma, S.; Virk, K.; Sharma, K.; Bose, S.K.; Kumar, V.; Sharma, V.; Focarete, M.L.; Kalia, S. Preparation of gum acacia-poly (acrylamide-IPN-acrylic acid) based nanocomposite hydrogels via polymerization methods for antimicrobial applications. *J. Mol. Struct.* **2020**, *1215*, 128298. [[CrossRef](#)]
255. Ji, X.-J.; Cheng, Q.; Wang, J.; Zhao, Y.-B.; Han, Z.-Z.; Zhang, F.; Li, S.-Q.; Zeng, R.-C.; Wang, Z.-L. Corrosion resistance and antibacterial effects of hydroxyapatite coating induced by polyacrylic acid and gentamicin sulfate on magnesium alloy. *Front. Mater. Sci.* **2019**, *13*, 87–98. [[CrossRef](#)]
256. Arik, N.; Inan, A.; Ibis, F.; Demirci, E.A.; Karaman, O.; Ercan, U.K.; Horzum, N. Modification of electrospun PVA/PAA scaffolds by cold atmospheric plasma: Alignment, antibacterial activity, and biocompatibility. *Polym. Bull.* **2019**, *76*, 797–812. [[CrossRef](#)]
257. Dil, N.N.; Sadeghi, M. Free radical synthesis of nanosilver/gelatin-poly (acrylic acid) nanocomposite hydrogels employed for antibacterial activity and removal of Cu (II) metal ions. *J. Hazard. Mater.* **2018**, *351*, 38–53. [[CrossRef](#)] [[PubMed](#)]
258. Doppalapudi, S.; Jain, A.; Khan, W.; Domb, A.J. Biodegradable polymers—an overview. *Polym. Adv. Technol.* **2014**, *25*, 427–435. [[CrossRef](#)]
259. Ranjbari, E.; Bazgir, S.; Shirazi, M.M.A. Needleless electrospinning of poly (acrylic acid) superabsorbent: Fabrication, characterization and swelling behavior. *Polym. Test.* **2020**, *84*, 106403. [[CrossRef](#)]
260. Mallawarachchi, S.; Mahadevan, A.; Gejji, V.; Fernando, S. Mechanics of controlled release of insulin entrapped in polyacrylic acid gels via variable electrical stimuli. *Drug Deliv. Transl. Res.* **2019**, *9*, 783–794. [[CrossRef](#)]
261. Shen, L.; Zhang, Y.; Yu, W.; Li, R.; Wang, M.; Gao, Q.; Li, J.; Lin, H. Fabrication of hydrophilic and antibacterial poly (vinylidene fluoride) based separation membranes by a novel strategy combining radiation grafting of poly (acrylic acid)(PAA) and electroless nickel plating. *J. Colloid Interface Sci.* **2019**, *543*, 64–75. [[CrossRef](#)]
262. Jose, J.; Shehzad, F.; Al-Harathi, M.A. Preparation method and physical, mechanical, thermal characterization of poly (vinyl alcohol)/poly (acrylic acid) blends. *Polym. Bull.* **2014**, *71*, 2787–2802. [[CrossRef](#)]
263. Yang, F.; Fan, X.; Zhang, M.; Wang, C.; Zhao, W.; Zhao, C. A template-hatched method towards poly (acrylic acid) hydrogel spheres with ultrahigh ion exchange capacity and robust adsorption of environmental toxins. *J. Ind. Eng. Chem.* **2019**, *69*, 422–431. [[CrossRef](#)]
264. Bin-Dahman, O.A.; Jose, J.; Al-Harathi, M.A. Compatibility of poly (acrylic acid)/starch blends. *Starch-Stärke* **2015**, *67*, 1061–1069. [[CrossRef](#)]
265. Das, D.; Ghosh, P.; Dhara, S.; Panda, A.B.; Pal, S. Dextrin and poly (acrylic acid)-based biodegradable, non-cytotoxic, chemically cross-linked hydrogel for sustained release of ornidazole and ciprofloxacin. *ACS Appl. Mater. Interfaces* **2015**, *7*, 4791–4803. [[CrossRef](#)]